LBL-23187

Lawrence Berkeley Laboratory
UNIVERSITY OF CALIFORNIA

Physics Division

AN ASTROMETRIC SEARCH FOR A STELLAR COMPANION TO THE SUN

S. Perlmutter
(Ph.D. Thesis)

November 1986

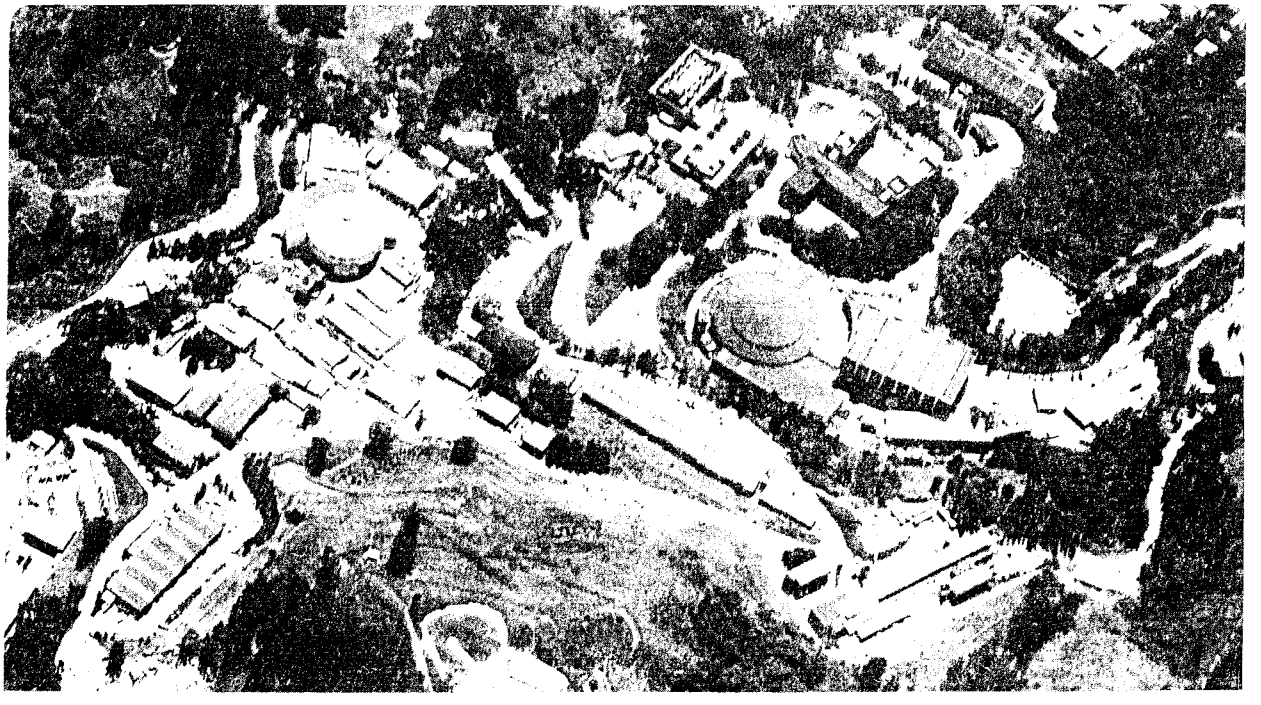

Prepared for the U.S. Department of Energy under Contract DE-AC03-76SF00098

An Astrometric Search for a Stellar Companion to the Sun

Saul Perlmutter

Lawrence Berkeley Laboratory
and
The University of California, Berkeley

Berkeley, CA 94720

Thesis submitted in partial satisfaction
of the requirements for
the degree of Doctor of Philosophy in Physics

25 November 1986

An Astrometric Search for a Stellar Companion to the Sun

Saul Perlmutter

Abstract

A companion star within 0.8 pc of the Sun has been postulated to explain a possible 26 Myr periodicity in mass extinctions of species on the Earth. Such a star would already be catalogued in the Yale Bright Star catalogue unless it is fainter than $m_v = 6.5$; this limits the possible stellar types for an unseen companion to red dwarfs, brown dwarfs, or compact objects. Red dwarfs account for about 75% of these possible stars. We describe here the design and development of an astrometric search for a nearby red dwarf companion with a six-month peak-to-peak parallax of $\geq$2.5 arcseconds. We are measuring the parallax of 2,770 candidate faint red stars selected from the Dearborn Observatory catalogue.

An automated 30-inch telescope and CCD camera system collect digitized images of the candidate stars, along with a $13' \times 16'$ surrounding field of background stars. Second-epoch images, taken a few months later, are registered to the first epoch images using the background stars as fiducials. An apparent motion, m_a, of the candidate stars is found to a precision of $\sigma_{m_a} \approx 0.08$ pixel $\approx$ 0.2 arcseconds for fields with $N_{fiducial} \geq 10$ fiducial stars visible above the background noise. This precision is sufficient to detect the parallactic motion of a star at 0.8 pc with a two month interval between the observation epochs. Images with fewer fiducial stars above background noise are observed with a longer interval between epochs. If a star is found with high parallactic motion, we will confirm its distance with further parallax measurements, photometry, and spectral studies, and will measure radial velocity and proper motion to establish its orbit.

We have demonstrated the search procedure with observations of 41 stars, and have shown that none of these is a nearby star.

Acknowledgements

I would like to thank the people who have contributed to this research work. My research advisor, Rich Muller, has shown me that it is possible to do top-quality physics without narrowing one's range of interests. The Nemesis hypothesis, on which this work is based, is but one example of the fruitfulness of his approach. Luis Alvarez, his thesis advisor, has taught me the ingredients necessary to get results in science: perceptive questions and a determination to find the answers.

My thesis committee members have played roles in my graduate career well before I began my thesis. Buford Price gave me my first stimulating introduction to forefront physics research. Walter Alvarez has offered me glimpses of a different science frontier, the geological past.

My work builds on the efforts of the entire Nemesis/Supernova Search team within the Lawrence Berkeley Laboratory astrophysics group. Carl Pennypacker has led these searches with optimistic enthusiasm. Jordin Kare and Shane Burns lay the groundwork for the automated telescope, CCD, and image analysis system in their doctoral work, and Roger Williams wrote much of the original software. Frank Crawford analyzed the optics and the CCD performance. When the day-

to-day work threatened to degenerate into pure computer programming, James Graham helped restore the focus on physics. Peter Friedman has shared with me many hours of work and discussion throughout our graduate careers.

I thank Terry Mast for his insightful advice on the data analysis, and particularly for his constructive criticism of the drafts of this thesis.

Throughout my work, my parents, Daniel and Felice Perlmutter, have provided unceasing support and encouragement.

This work was supported in part by the Department of Energy under contract DE-AC03-76SF00098.

Table of Contents

1. Introduction

Binary Stars

Studies of binary stars suggest that more than 84% of solar-type stars are in binaries (Abt, 1983). The sun has generally been considered one of the exceptions, since the past century's cataloging of nearby stars has failed to discover a companion star bound to the sun. Occasional articles have proposed that a nearby star may have escaped detection or identification as a solar companion. Van de Kamp (1982), for example, in discussions on wide-binary pairs suggests that a wide-binary companion could have been missed in the current catalogues. In response to the new observational capabilities of IRAS and the Hubble Space Telescope, Reynolds, Tarter and Walker (1980) also discuss the possibility of finding an unseen faint companion. These proposals have not yet been followed through; there has been no concerted all-sky search for a solar companion.

Extinctions

Recently, evidence from the more earthbound fields of paleontology, geology, and geophysics has excited renewed interest in a solar companion. The background was set by the proposal of L. Alvarez *et al.* (1980) that the Cretaceous-Tertiary extinction was caused by the impact on the earth of a large comet or asteroid. Since comets and asteroids are known to have a higher concentration of iridium than the Earth's crust, this theory explained the anomalously high con-

centration of iridium in the clay layer that marks the Cretaceous-Tertiary boundary.

The impacts could cause the mass extinction through a number of possible mechanisms. L. Alvarez *et al.* (1980) suggested that the impact would raise enough particulate matter into the atmosphere to block the sunlight reaching the earth. This would interrupt photosynthesis in the biosphere, the food chain on earth would be disrupted, and entire families of species would become extinct. Toon *et al.* (1982) pointed out that the opaque atmosphere would also produce sub-freezing temperatures on the continents, causing extinctions of many land animals. This scenario has been discussed in recent "nuclear winter" analyses of the outcome of a large-scale nuclear war (Turco *et al.*, 1983).

Since Alvarez *et al.* first proposed the impact explanation for the Cretaceous-Tertiary extinction, substantial evidence has been collected supporting the correlation between impacts and mass extinction events. The high concentration of iridium at the extinction boundary has been found to be distributed world-wide. Iridium has also been found in concentrations above the background at other extinction boundaries besides the Cretaceous-Tertiary. At many of these boundary sites there is shocked quartz, which is found at known impact sites, and mineral spherules (probably altered microtektites), which could have originated as droplets of impact melt. Alvarez (1986) reviews this and other evidence.

Periodic Extinctions and a Solar Companion

The theoretical situation became more complicated when Raup and Sepkokski (1984) reported evidence for a 26 million year periodicity in the fossil record of mass extinctions on the earth; the Cretaceous-Tertiary extinction fit the phase of the periodicity. This periodicity was difficult to reconcile with the cometary impact theory, since impacts were considered rare and random occurrences. In response to this theoretical difficulty, Davis, Hut and Muller (1984) and Whitmire and Jackson (1984) independently suggested that a solar companion could cause periodic comet showers on the earth. Other explanations for the periodic extinctions were also proposed (Whitmire and Matese, 1985; Rampino and Stothers, 1984), but they fail to be supported by further analysis (Muller, 1985).

The solar-companion model of Davis, Hut and Muller proposes a star in an orbit about the sun with an eccentricity $e \geq 0.7$, and a semi-major axis a chosen to give a period $T = 26$ Myr:

$$a\ [\mathrm{AU}] = (T\ [\mathrm{yr}])^{2/3}$$

$$= 8.8 \times 10^4\ \mathrm{AU}\ = 0.43\ \mathrm{pc} \qquad (1)$$

where the units have been chosen such that Kepler's constant $k \equiv T^2/a^3 = 1$. Every 26 Myr, when this star passes through perihelion, its gravitational field randomizes the motions of the 10^{11}—10^{13} comets in the Oort cloud, currently thought to orbit the sun at distances up to ~10^5 AU. Hut (1985) has shown using numerical simulations that the Companion star mass must be $\geq 0.06 M_\odot$ to perturb the motions of the Oort cloud comets.

With each close passage of the Companion, some of the perturbed comets will enter the inner solar system, which is usually kept clear of comets by the sweeping action of Jupiter's gravitational field. Davis, Hut and Muller estimate that during each of these periods of cometary presence in the inner solar system an average of 2-25 comets will hit the earth, causing periodic mass extinctions. (The name they suggested for the star, Nemesis, seems appropriate.)

Other Evidence

The discovery of periodicity in the dates of craters on the earth has provided the strongest supporting evidence for periodicity. Alvarez and Muller (1984) found a 28.4 $\pm$ 1.0 Myr periodicity that corresponds to Raup and Sepkokski's extinction periodicity within the errors of the geologic time scale. Rampino and Stothers (1984) and Shoemaker (1985) used slightly different sets of craters and found respectively a 31 Myr periodicity and a 30 Myr periodicity. These results differ mostly in the phase of the most recent events, since the earlier time scale is uncertain enough to allow cycles of differing frequency to match. It is also important to note that if a Companion Star's orbit is the ultimate cause of the periodicity, then the comet showers are expected to be only approximately periodic. Hut (1984) has shown that the Companion's orbit is expected to be perturbed by passing stars and the Galactic tidal field, and thus the period between impacts should vary by 10%-20%.

This Search

The evidence supports the claim that periodic impacts on the earth have caused mass extinctions. It does not show that the periodic comet showers are caused by the close passage of a solar companion. The most incontrovertible evidence would be the discovery of a companion star with the appropriate orbital period. We are now searching for such a companion star, and hope to finally discover if the Sun is a member of a binary system. We describe here the design and development of an observational program to measure the parallax, and hence the distance, of candidate stars in the northern hemisphere.

2. Choice of Search List

2.1. Astrophysical Constraints on a Solar Companion

For a star orbiting the sun with semi-major axis $a = 0.43$ pc and eccentricity $e = 0.7$, the maximum distance from the sun will be

$$r_{\max} = (1+e)\,a = 0.73 \text{ pc} \tag{2}$$

Using numerical simulations Hut (1985) found that the Galactic tidal field slightly increases the a and $r_{\max}$ necessary for a $T = 26$ Myr orbit. He obtained $r_{\max} = 0.8$ pc. The six-month peak-to-peak parallactic motion at this distance is

$$\theta_{p-p}[\text{arcsec}] = \frac{2}{r_{\max}[\text{pc}]} = 2.5 \text{ arcsec} \tag{3}$$

(The conventional definition of *parallax* is half of this peak-to-peak motion: $\pi \equiv \theta_{p-p}/2 = 1.25$ arcseconds.) This is the *minimum* motion we could expect for a Companion, obtained if we are presently halfway between two perihelion passages, as evidenced by mass extinctions. Since this phase is not certain, the Companion could be closer and have a higher parallax. Using this limiting value for the Companion's distance, we can ask how current astrophysical knowledge constrains the attributes of a solar companion.

Proper Motion Surveys

Surprisingly, little information can be gleaned from the catalogues of nearby stars, because these stars are mostly discovered in surveys for large proper

motion. For a star bound to the sun with a 26 Myr periodicity, the proper motion, μ, at r_{max} will be

$$\mu(r_{max}) = \frac{v(r_{max})}{r_{max}}$$

$$\approx 0.01 \text{ arcsec/yr} \qquad (4)$$

This is well below the $\mu = 0.18$ arcsec/yr limit set by the Luyten Catalogue complete sky survey (Luyten, 1979;1980). The proper motion is larger at closer distances, but only exceeds the $\mu = 0.18$ arcsec/yr limit when the companion is near perihelion. The parallactic motion, $\theta_{p-p} = 2.5$ arcseconds, for a companion star at $r_{max} = 0.8$ pc *will* be above the Luyten Catalogue limit. However, the proper motion surveys use observations collected at the same time of year for both epochs, and therefore are not sensitive to parallactic motion.

The Yale Bright Star Catalogue

Even at r_{max}, the Solar Companion would be the closest star in the sky, and the brightest star of its spectral type and luminosity class. The Yale Bright Star Catalogue (Hoffleit, 1982) is complete to apparent magnitude $m_v = 6.5$, and no star in the catalogue has the parallax, proper motion, or spectroscopic parallax consistent with the orbit of a Solar Companion. This constrains a Solar Companion to be among a small set of stellar types. Figure 1 shows the Yale Catalogue's brightness limit on the H-R diagram. Any star within 1 pc would be contained in the Yale Catalogue if its stellar type lies above the line at apparent magnitude

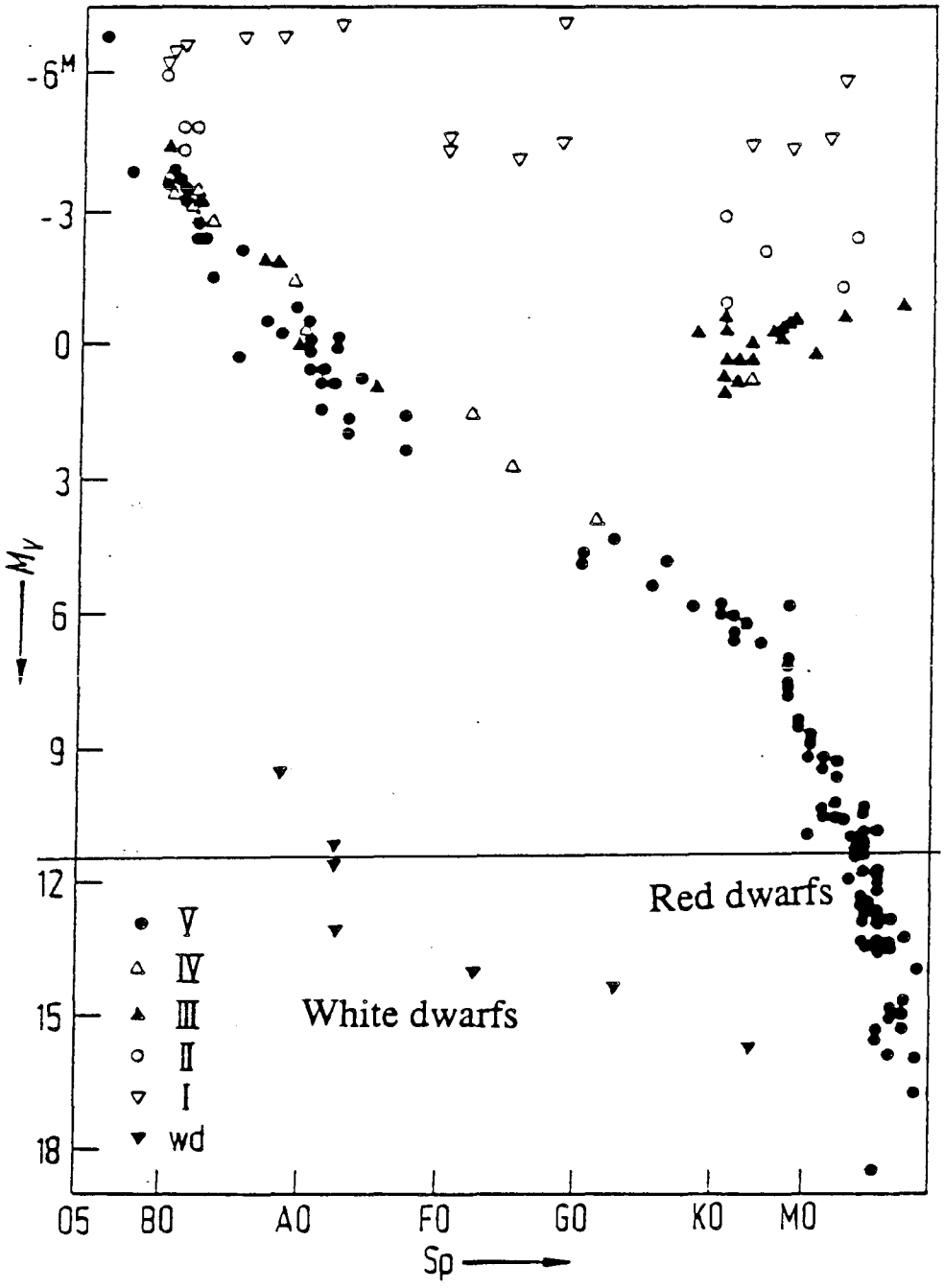

Figure 1

The Hertzsprung-Russell diagram for the 100 nearest stars and the 100 closest stars (Schaifers and Voigt, 1982). The Yale Bright Star Catalogue's completeness limit is indicated by the horizontal line.

$m_v = 6.5$, or absolute magnitude $M_v = 11.5$. Thus a companion star, if it exists, must be a red dwarf, white dwarf, or one of the stellar types not shown on Figure 1, the brown dwarfs, neutron stars, and black holes.

2.2. Companion Star Search

Red Dwarf Stars

Of these possible stellar types, we have chosen to search for a red dwarf companion. Much work has already been done by the Dearborn Observatory's survey for faint red stars (Lee *et al*, 1943, 1944, 1947; Nagy, 1979), which has cataloged all of the red stars in the northern hemisphere to a limiting magnitude for late M dwarfs of $m_v \approx 13$ (Stevenson, 1984). (No comparable survey has been done for the southern hemisphere.) As can be seen in Figure 1, this Dearborn Observatory Catalogue would include any red dwarf star within 1 pc. This catalogue does not distinguish, however, between red dwarf and red giant stars, and thus the problem is reduced to finding the nearby dwarfs among the many distant giants. We have developed an astrometric parallax search to find a nearby star if it is in the Dearborn Observatory Catalogue. This search is clearly only a first attempt to find a Companion with the highest chance of success for the least effort, since the Companion could be in the southern hemisphere and/or may not be a red dwarf.

Other Stellar Types

There is no *a priori* expectation that a solar companion should be of a certain stellar type. A search of just the red dwarfs does, however, include most known stars. Table 1 shows the Luminosity Function of Bahcall and Soneira (1980), which gives the number of stars per cubic parsec in each magnitude interval. We find that ~54% of all known stars are red dwarfs below the Yale Bright Star Catalogue $M_v = 11.5$ limit. Only ~4% are stars massive enough to become white dwarfs, neutron stars, or black holes in the $T_\odot \approx 4.5 \times 10^9$ year lifetime of the Sun. Extrapolating back in time 4.5 billion years increases the proportion of massive stars only slightly to ~5%. Thus there are about 0.1 times as many compact object (white dwarf, neutron star, or black hole) candidates as red dwarf candidates.

The proportion is less clear for brown dwarfs, which have not yet been found, but are postulated to exist with masses $<0.08\ M_\odot$. These stars are not massive enough for hydrogen burning in the core, and thus are expected to have low luminosities. Bahcall (1986) has suggested that the missing mass in the galaxy may consist of unseen brown dwarfs. If all of the missing mass, $\rho_{missing} = 0.10 \pm 0.05\ M_\odot\ pc^{-3}$, is in the form of brown dwarfs with mass less than $0.08\ M_\odot$, but greater than the $0.06\ M_\odot$ necessary for a Companion to perturb the Oort cloud, then the brown dwarfs would account for >95% of the stars that could be a Companion. This is not likely, since there is no reason to believe that the bulk of brown dwarfs would not have masses closer to $0.001\ M_\odot$, partic-

Table 1

The luminosity function for
all stellar types in the Galaxy
(after Shapiro and Teukolsky, 1983)

M_v	Luminosity Function $\phi(M_v)$ (stars $pc^{-3}mag^{-1}$)	Mass $M/M_\odot$	Lifetime on Main Sequence log T_{MS} (yr)	
-6	1.49×10^{-8}	117.5	6.42	
-5	7.67×10^{-8}	63.1	6.50	
-4	3.82×10^{-7}	33.9	6.58	
-3	1.80×10^{-6}	18.2	6.84	
-2	7.86×10^{-6}	9.8	7.19	
-1	3.07×10^{-5}	5.2	7.68	
0	1.04×10^{-4}	2.8	8.36	
1	2.95×10^{-4}	2.3	8.62	
2	6.94×10^{-4}	1.8	8.93	
3	1.36×10^{-3}	1.5	9.24	
4	2.26×10^{-3}	1.2	9.60	$T_{MS} \leq T_\odot$
5	3.31×10^{-3}	0.95	9.83	
6	4.41×10^{-3}	0.78	10.28	
7	5.48×10^{-3}	0.63	—	
8	6.52×10^{-3}	0.51	—	
9	7.53×10^{-3}	0.41	—	
10	8.52×10^{-3}	0.33	—	
11	9.54×10^{-3}	0.27	—	
12	1.06×10^{-2}	0.21	—	M_v
13	1.17×10^{-2}	0.17	—	below
14	1.29×10^{-2}	0.14	—	Yale Catalog
15	1.41×10^{-2}	0.11	—	limit
16	1.41×10^{-2}	0.09	—	

ularly if the Luminosity Function continues, as in Table 1, to rise with decreasing mass. If we estimate that there is approximately the same density of stars in the 0.06—0.08 $M_\odot$ mass bin as in the 0.08—0.10 $M_\odot$ mass bin of Table 1, we find that there would be ~0.23 as many brown dwarf Companion candidates as red dwarf candidates. Considering red dwarf, compact object, and brown dwarf candidates, our search of red dwarfs thus includes $(1 + 0.1 + 0.23)^{-1} = 0.75$ of the possible candidates in the northern hemisphere.

2.3. The Search List

We have selected stars from the Dearborn Observatory Catalogue of Faint Red Stars to be the candidates for the search. Only stars that lie below the $m_v = 6.5$ limit shown on Figure 1 are placed on the Search List. This limits us to a subset of the red dwarfs, those with spectral types cooler than M4. The Dearborn Observatory Catalogue contains 5,518 stars of types M4-M9. This is expected to be a complete list of the hydrogen-burning cool stars that are candidates within 1 pc in the northern hemisphere.

Magnitude-Color Relation

We use the "main sequence" correlation between spectral type and absolute magnitude (shown in the first two columns of Table 2) to further trim our Search List. Many stars within the M4-M9 subset are too faint to be stars of their spectral type within 1 pc of the Sun. Taking into account the ~0.5 magnitude uncertainty of the Dearborn Catalogue, we eliminate 2,748 stars using the brightness

criterion listed in the fourth column of Table 2. Figure 2 shows which stars these cuts remove from the Dearborn Observatory Catalogue. The Companion Search thus begins with a Search List of 2,770 candidate stars.

Table 2

Cuts used on the
Dearborn Observatory Catalogue

Spectral Type	$M_v^{(a)}$	m_v at 1 pc	m_v cut used	number cut	number remaining
M4	11.3	6.3	8.0	2005	440
M5	12.3	7.3	10.0	743	936
M6	13.5	8.5	—	0	933
M7	14.3	9.3	—	0	395
M8	16.0	11.0	—	0	63
M9+	—	—	—	0	3
			Totals:	2748	2770

[a] M_v from Schaifers and Voigt (1982)

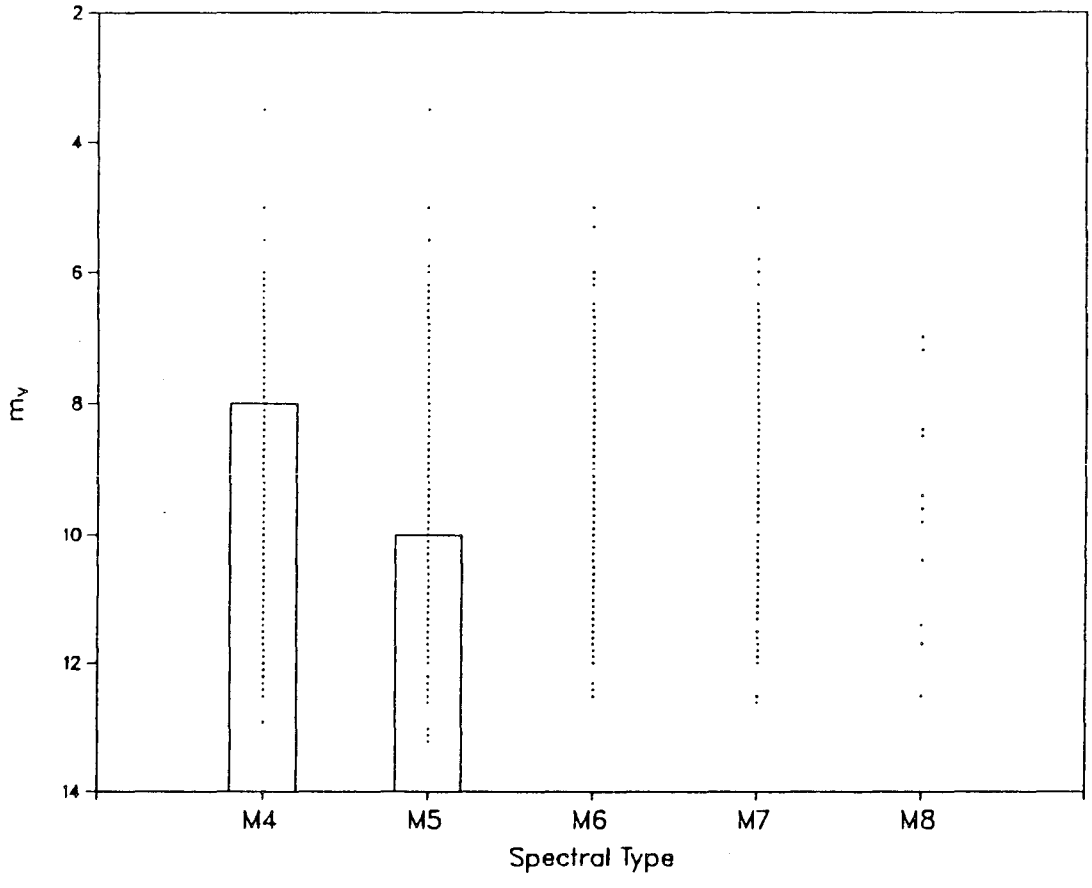

Figure 2

Scatterplot of Dearborn Observatory Catalogue stars of spectral types M4—M8. Boxes show faint stars deleted from the Search List.

3. Data Collection

3.1. Overview

The goal of the search is to discover any star on the Search List with a parallactic motion greater or equal to 2.5 arcseconds peak-to-peak. The search procedure is as follows: Every night with available telescope time, we observe a subset of stars from the Search List. Images are collected with a CCD camera, digitized, and recorded on magnetic tape. These tapes are later read into the lab computer and analyzed. If any image is overexposed, underexposed, out of focus, or otherwise unusable the Search List is updated with corrected observation parameters (e.g. exposure time) for a new observation. For usable images, the analysis program finds the stars in the image, both the Search List star and the background stars, and writes the coordinates and description of each star into a data base.

When a sufficient number of months has passed for us to be able to detect parallactic motion, we re-observe the stars, and compare the first epoch coordinates to the second epoch coordinates for each star field. Using the background stars to "register" the two images with each other, we find the overall offset, rotation and magnification changes between the two images. Taking these changes into account we calculate the apparent motion, m_a, of the Search List star. Any star with a small m_a is removed from the Search List and no longer considered a Companion Star candidate. Any star with significant m_a is subjected to close

scrutiny, reobservation, and reanalysis as a possible Companion candidate. Figure 3 charts this process for the second-epoch observation.

The Companion Star Search shares much of its procedure and equipment with the Berkeley Supernova Search. Detailed descriptions of the telescope, automation, camera, and data path can be found in Burns (1985), Kare (1984), and Kare *et al.* (to be published). The remainder of this chapter will describe the details of the Companion Star Search procedure. The data analysis will be discussed in the following chapter.

3.2. Generating an Observation List

For each night's observations, we select stars from the Search List to create an Observation List. We take a number of factors into account in making this selection:

Atmospheric Dispersion

The stars on our Search List are red, while the typical background stars in our exposures are hotter, with a black-body peak in the yellow part of the spectrum. If the two epochs' images are taken at different zenith angles, we will measure a non-zero m_a for a Search List star with respect to the background stars, because of the atmospheric dispersion of the different colors. We attempt to observe both epochs at the same zenith angle, but it is difficult to schedule the second-epoch observations at just the times of night when the zenith angles agree.

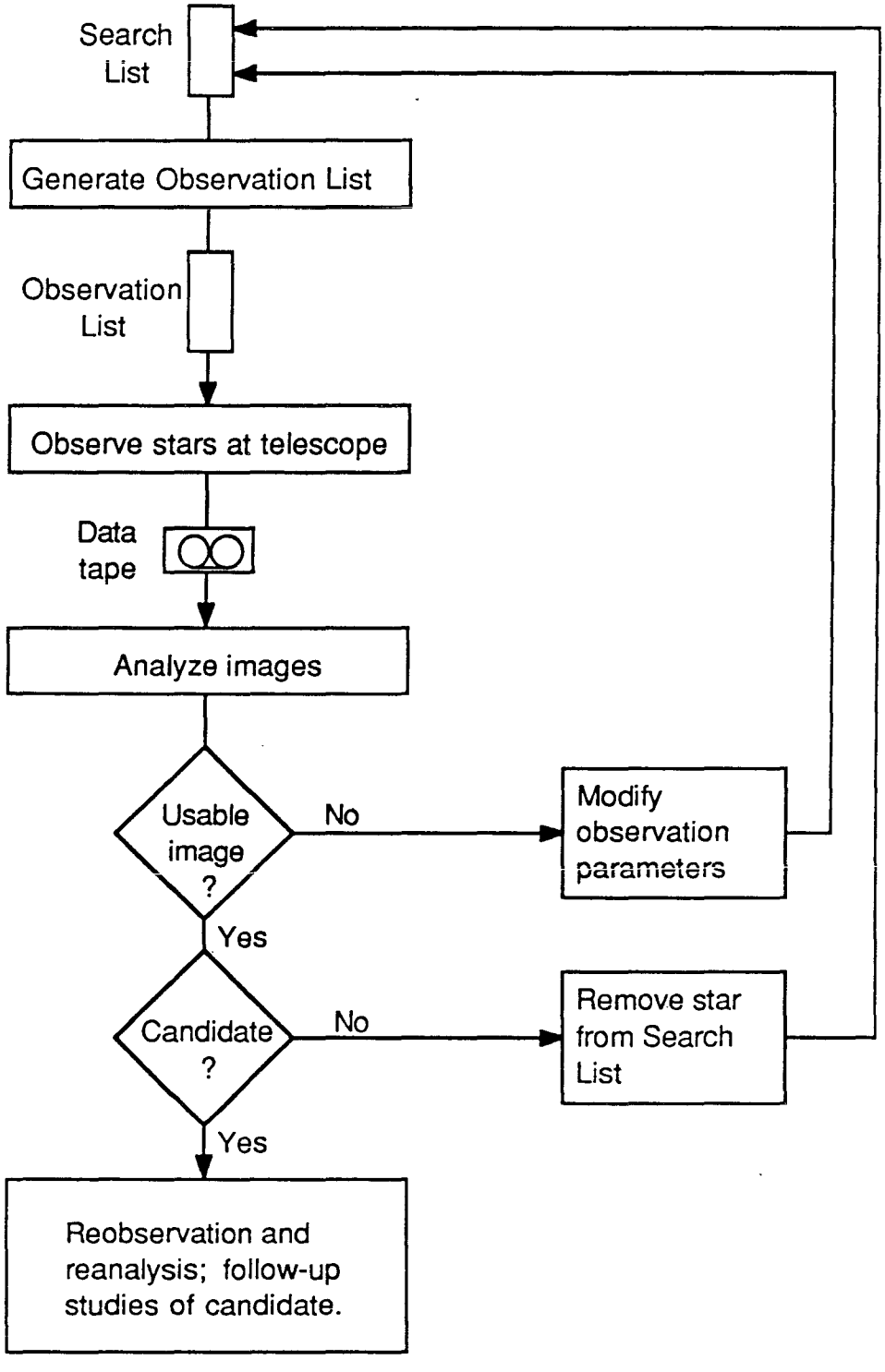

Figure 3

Flowchart for second-epoch observation and analysis.

We therefore try to take the exposures at small zenith angles to minimize the dispersion. For the Observation List, we select stars that will be near the zenith at the time of both the first and second epoch observations.

Parallactic Motion

Even if all of the stars on the Search List were at 0.8 pc, they would not all appear to move the same distance between two arbitrary dates of observation. We can maximize the parallactic motion by choosing observation dates for a given star according to its location on the "celestial sphere." In particular, stars which are at low ecliptic latitudes—coplanar with the earth's orbit—appear to trace out a sinusoid in Right Ascension versus time, making it necessary to choose observation dates with care. They reach their maximal excursions when they are just visible at dusk and at dawn, but move fastest at the midpoint between these two dates, when they are directly overhead at midnight.

Stars at high ecliptic latitudes on the other hand can be observed most of the year, since they trace out circles in the sky annually; this motion can be measured at any two points sufficiently far around the circle. In selecting candidates for the Observation List, we therefore first choose stars that are at low latitudes and are about to exhibit their greatest parallactic speed in the following few months. The remainder of a night's Observation List can then be filled with the high-latitude stars, for which the observation dates are less important.

Dewar Configuration

The telescope cannot be pointed above 58° in declination unless the liquid-nitrogen dewar (used to cool the CCD) is mounted at an angle allowing it to clear the telescope's supporting fork. At this angle the dewar cannot be completely filled with liquid nitrogen, so it is usually mounted in a more perpendicular position. Thus depending on how the dewar will be mounted on a given night, stars over 58° are either preferentially included or excluded from the night's observation list.

Seeing Limitations

Some selections are based on the seeing at the time of observation. If the seeing is poor, stars are spread over more pixels and therefore brighter stars, which would otherwise saturate the image, can be safely added to the list. We prepare alternate observation lists for different seeing conditions.

Observation List Contents

An Observation List contains the following data for each star:

a) Dearborn Observatory Catalogue number
b) Coordinates: RA and Dec.
c) Spectral type: M4, M5, ..., M8
d) Apparent magnitude, m_v
e) Exposure time (seconds)
f) Sequence number on the Observation List

3.3. Observations

The search employs the 30-inch Ritchey-Chrétien reflector telescope at the University of California's Leuschner Observatory (longitude 122.157°, latitude 37.918°). Dr. R. Treffers, of the Berkeley Astronomy Department, has extensively automated the Leuschner facility, and the Lawrence Berkeley Laboratory's astrophysics group has improved the telescope speed and pointing accuracy, and the on-line computing resources. While minor refinements and major upgrades are continually changing the operation of the telescope, the current system is sufficiently evolved to carry out the Companion Star Search. Figure 4 shows a block diagram of this system.

For the Companion Star Search, the goal of the data collection is to image each star field on the CCD camera and record the image. (The plate scale is 2.4 arcseconds per CCD pixel. One pixel thus roughly corresponds to the typical seeing at the telescope, 3 arcseconds, and to the parallactic motion of a companion at 0.8 pc, $\theta_{p-p} = 2.5$ arcseconds.) An IBM XT controls most of the operations, making it possible to collect hundreds of such images each night. Using the observation parameters for a star from the observation list, the XT points the telescope, and opens and closes the shutter. It then reads out the CCD camera's digitized data onto videotape, adding bookkeeping information describing the observation onto the tape's audio track. This process is repeated until the observation list is exhausted.

With ideal camera, optics, and software, this simple repetitive procedure

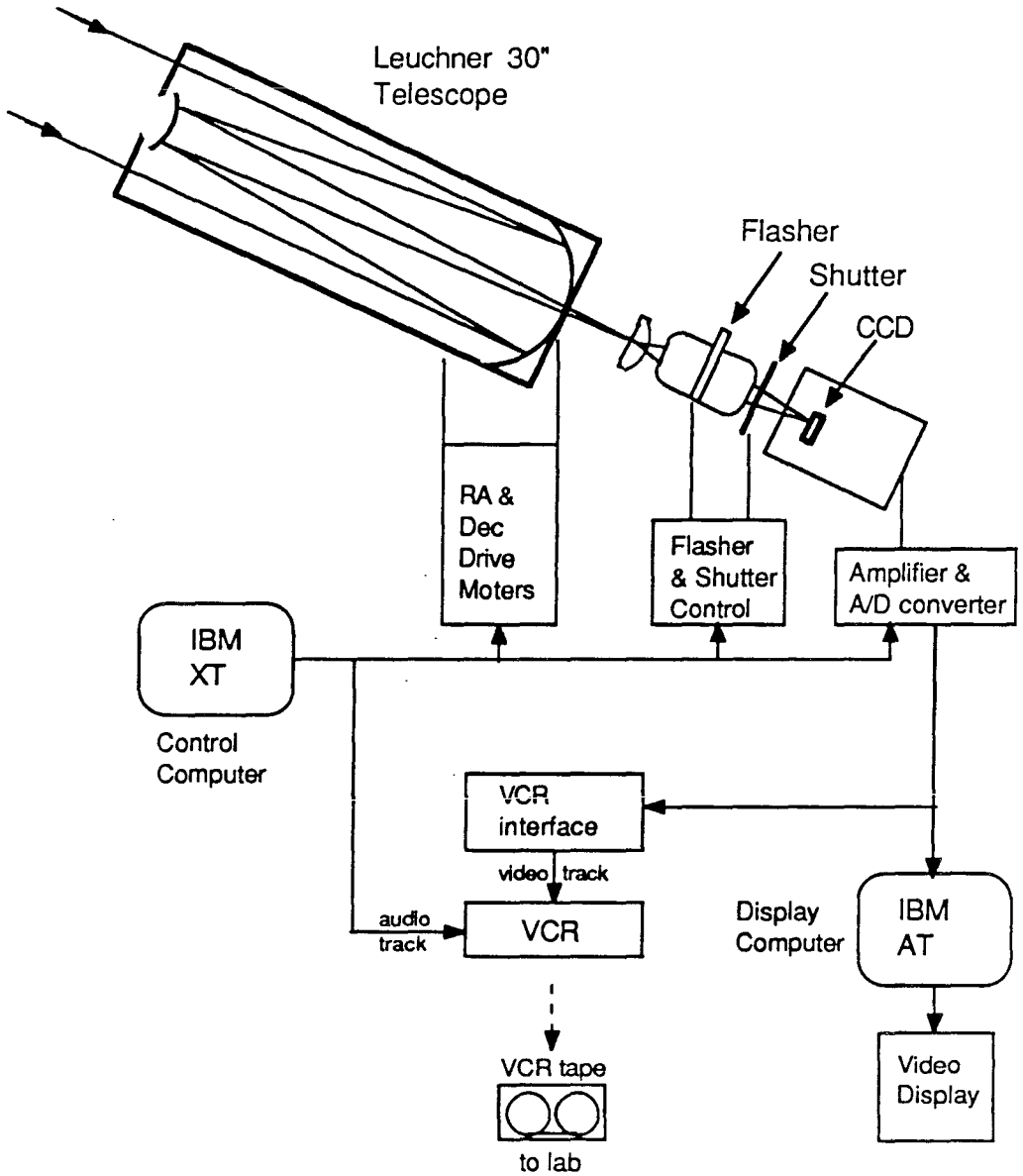

Figure 4

Block diagram of current observatory system.

would suffice to achieve the precision we desire for our final results. In practice, some additional steps are required both before an observation list is begun, and during the observation of each star.

Telescope Pointing

Since the optics that focus the light from the telescope onto the CCD are not ideal, some vignetting and pincushion distort the final image. The vignetting reduces the amount of light at the top of the CCD frame to less than half of the light in the middle of the frame. The pincushion distortion moves images radially by $\Delta r = p_0 r^3$, where the constant of proportionality for our optics is $p_0 \approx 6.5 \times 10^{-8}$ pixels^{-2}. These distortions shift the apparent positions of stars, a larger shift occurring for stars that lie further from the center of the image. We cancel this effect by pointing the telescope so that the position of the second-epoch image on the CCD's pixels matches the position of the first-epoch image.

The telescope pointing algorithm is initialized while the telescope is imaging a fiducial star of known coordinates on the center of the CCD's pixel array. To locate the fiducial star image within a few pixels of the array center, we send the digitized image to an IBM AT computer, which has a Tecmar graphics display card. Here we can display the image on a composite-video monitor, and manually move a superposed cursor to determine a star's position to within one pixel. For the first-epoch observations, a catalogued bright star with well-determined coordinates is used as a fiducial. It is placed within three pixels of the center pixel for

the initial telescope pointing, and in the course of the night the pointing will stay within about 6 pixels RMS. For the second-epoch exposures, a star seen in a matching first-epoch image is used as the fiducial.

"Flashing" the CCD

The CCD detector is itself not an ideal instrument. It operates by collecting photoelectrons that photons knock out of its substrate into an array of 320×512 potential wells. The amount of charge collected in each potential well thus represents the amount of light that has fallen on that pixel. A bucket brigade of charge transfers brings each packet of charge down the columns and across the bottom row to a single amplifier at one corner of the array. The amplifier measures the charge in each pixel, and the result is then digitized by an analogue/digital (A/D) converter, with an overall gain of ~28 photoelectrons per A/D count.

The charge transfers in the bucket brigade are not perfectly efficient, and some fraction of the charge gets left behind at each transfer. For a star image, this causes a tail of inefficiently transferred charge to grow behind the peak as it moves across the CCD. A good CCD will have an inefficiency of less than $\epsilon=10^{-4}$, so that after the 832 transfers from the farthest corner of the CCD, the amount of charge left behind in the tails is only

$$1-(1-\epsilon)^{832} \approx 0.08 \qquad (5)$$

Measurements of the CCD, RCA model SID53612XO, by Burns (1985) yielded

transfer inefficiencies of

$$1.6\times10^{-4} < \epsilon < 5\times10^{-4}$$

for

$$-88\ ^{\circ}C > T_{CCD} > -130\ ^{\circ}C \tag{6}$$

where T_{CCD} is the operating temperature of the CCD.

More recently, we have found that the transfer efficiency of the CCD also depends strongly on the amount of charge being transferred. It is apparently harder to transfer the first electrons out of the potential wells, an effect which has been referred to as "fat zero" and "sticky bucket." The effect can clearly be seen in Figure 5, which shows the shapes of a bright star image and a dim star image. The dim star is in the high ϵ regime, and thus has grown a tail of inefficiently transferred charge as it was transferred from (Row 130, Column 254) to the amplifier at (0,0). The bright star is in the low ϵ regime, and thus has a round profile characteristic of efficient charge transfer.

A dim star with a tail will appear to have a centroid shifted toward higher coordinates. This effect can be seen in Figure 6(a), which shows results of measurements made in the lab, with a simulated star image held at one spot on the CCD for each curve. The apparent centroid for a star image is plotted against the brightness of the star, and the different curves show the effect of placing the star image at different distances form the amplifier corner. The apparent centroid of the star clearly shifts more as the star becomes dimmer, and the effect becomes more pronounced as the star image is moved away from the amplifier.

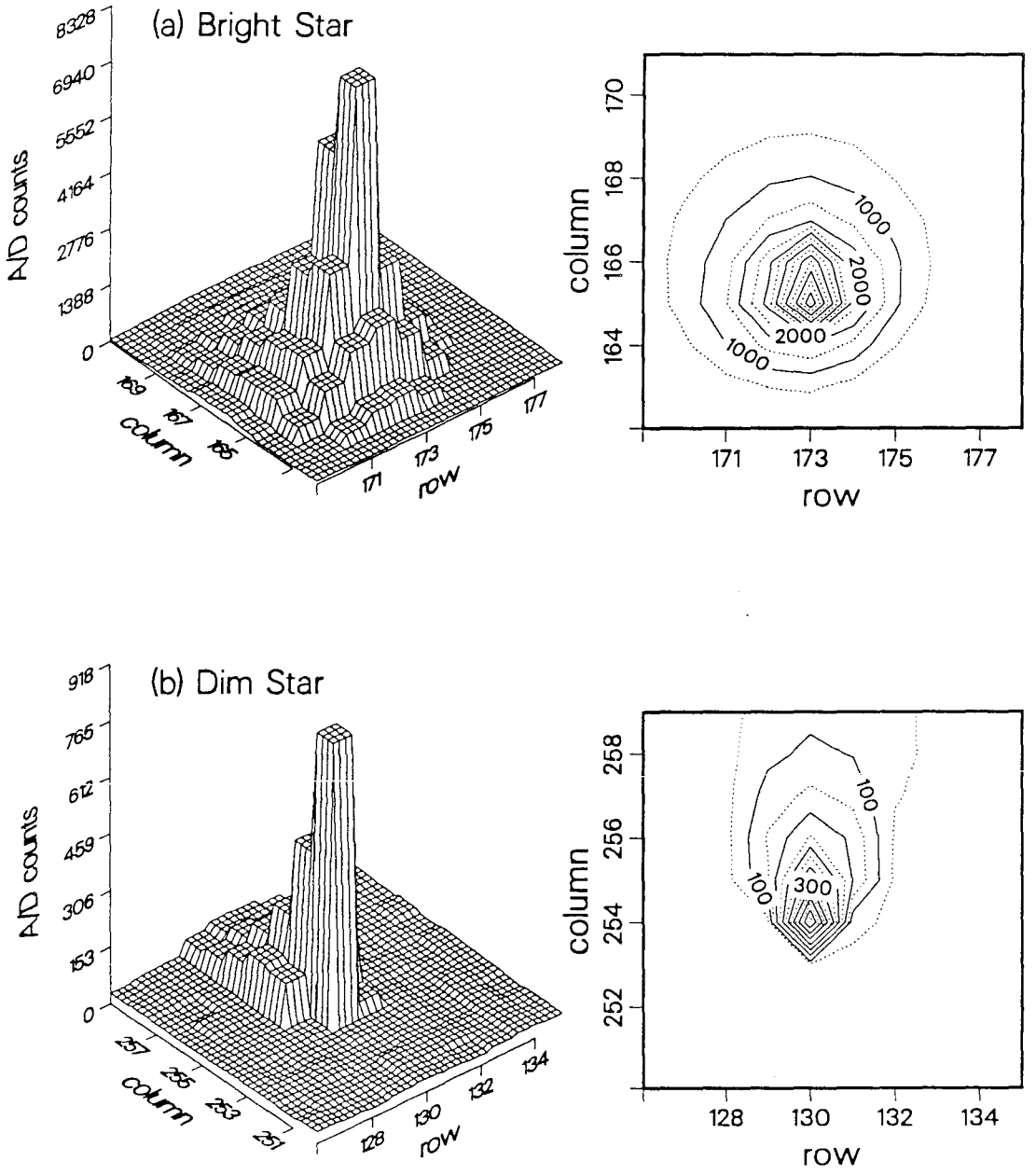

Figure 5

Two-dimensional histogram and contour plot, showing the number of photoelectrons in a box of 10×10 pixels containing (a) a bright star and (b) a dim star. The asymmetric tail of the dim star is due to CCD charge-transfer inefficiency.

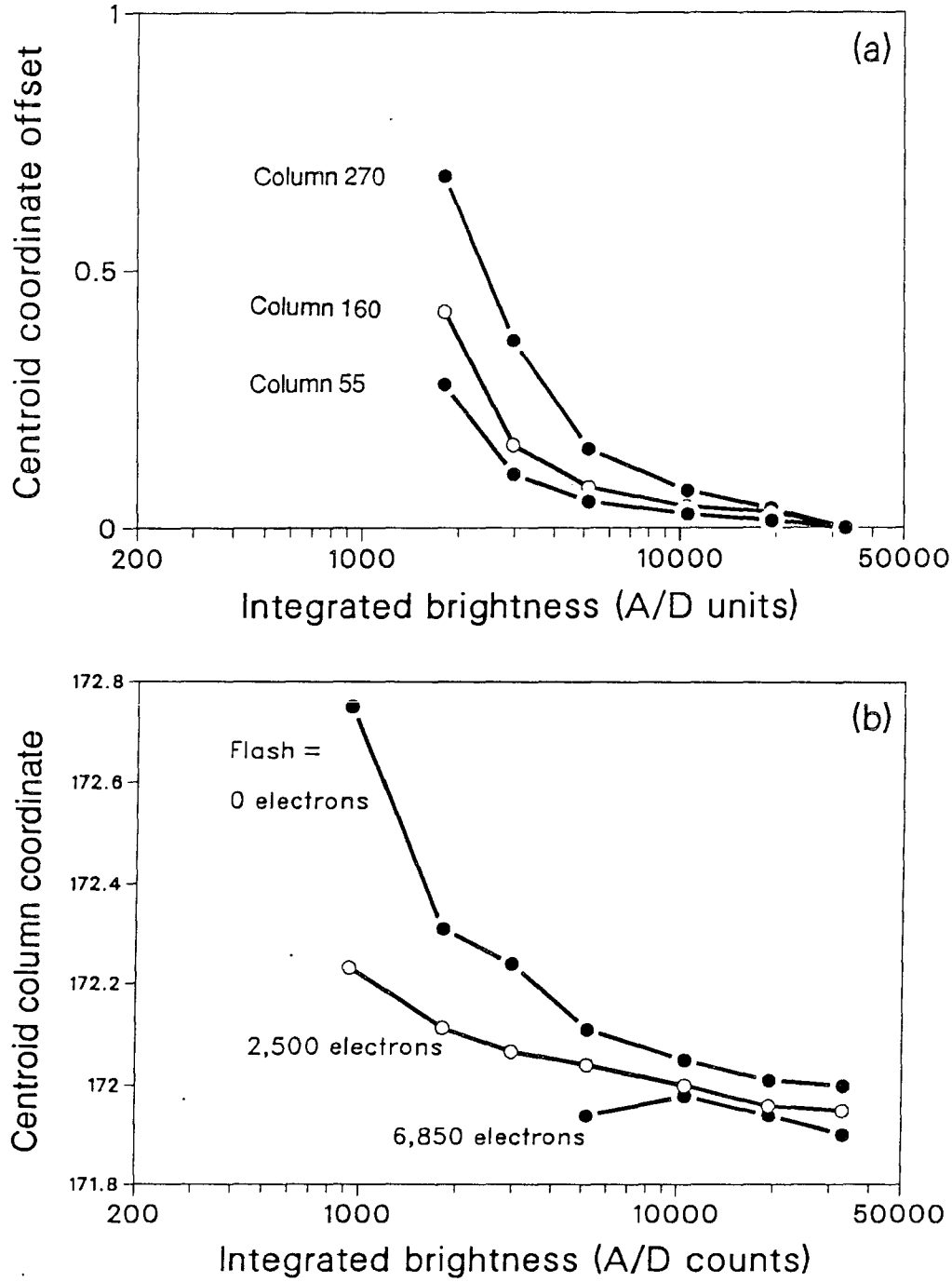

Figure 6

The effect of star brightness on charge-transfer inefficiency, shown by the change of centroid for a simulated star held at a fixed location on the CCD. (a) The curves show different locations on the CCD. (b) The curves show different levels of background light.

Since ϵ is a function of the amount of charge in a pixel, we can improve the shape of a dim star, and the accuracy of its centroid, by adding a flat field of background light to the image. Figure 6(b) again plots apparent star centroid against star brightness, but the three curves show that the effect is reduced by adding 2,500 electrons or 6,850 electrons of background light.

We ran computer simulations of a CCD transferring charge with an efficiency which depends on the amount of charge, in an attempt to model the shape of the images found on our CCD. Results indicate that the inefficiency varies from ϵ=10^{-2} to ϵ=10^{-4}, as the number of electrons in the potential well rises from zero to 20,000. Above this brightness the inefficiency approaches the values of Burns (1985), $1.6\times10^{-4} < \epsilon < 5\times10^{-4}$.

For the search observations, we want the improved transfer efficiency obtained with more electrons in the wells. We therefore designed a flash unit consisting of four LED's mounted in the corners of a frame, which can be inserted in the slot intended for color filters. This slot is out of focus in the parallel beam between the Bronica lens, which receives the focussed light from the telescope, and the Nikkor lens, which focuses the light onto the CCD. [For further details of the optical configuration, see Kare (1984).] A 1.3—2.0 second flash during each observation adds a diffuse background of 20,000—30,000 electrons, with a peak-to-valley spread in intensity of ~10%. This changes the faint star images read from the CCD from asymmetric "comets" to round stars. A measure of "roundness," R is defined to be

$$R \equiv 2\frac{\sigma_{Row} - \sigma_{Column}}{\sigma_{Row} + \sigma_{Column}} \tag{7}$$

where σ_{Row} and σ_{Column} are the widths of the best-fit gaussians in the row and column direction. We find that after flashing the typical faint star has a roundness $| R | < 0.2$.

We incorporate this flash into the observation cycle at two points. First, the IBM XT powers the flash unit, typically for 1.5 seconds each time the shutter is opened. Second, we intersperse a series of three calibration exposures approximately every twenty minutes of observation. These calibrations are a series of 1.5 second exposures of the flashed background plus three different dim star fields. By taking the median (not the average) of three exposures, we remove the star fields and obtain an image of the background light that each observation exposure has in common. Repeating the calibration exposures throughout the night provides a check for drift in the flash background pattern. We have found this pattern to be stable to within 1-2 pixels over the hour required for a typical observation list.

3.4. Future Improvements

A number of changes to the search procedure are being introduced as they are perfected. In the near term, we will begin using a DEC microVAX II computer, which has recently been installed at the telescope and networked to the existing system via Ethernet (see Figure 7). The microVAX will control the telescope pointing and the readout of the CCD camera through the existing IBM

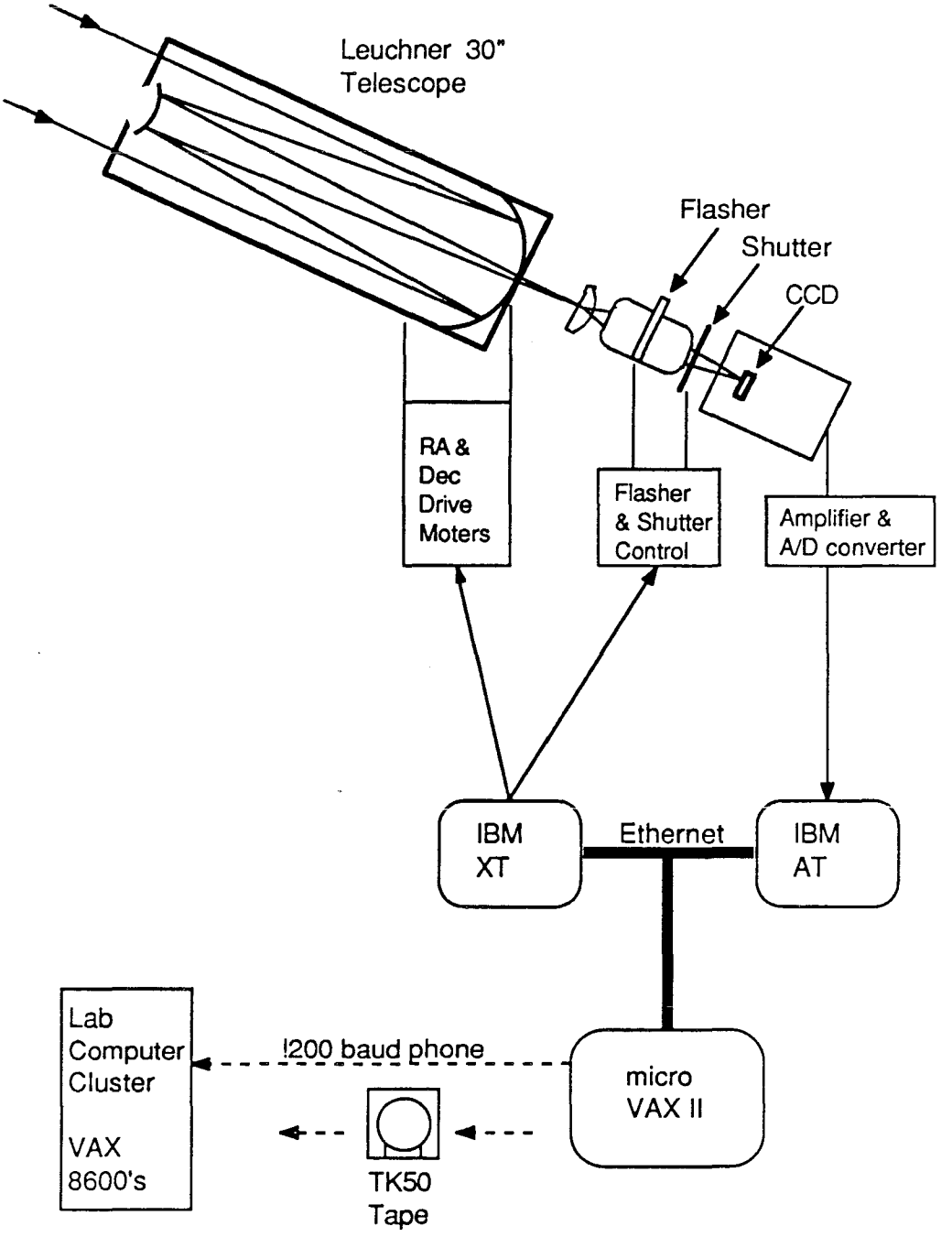

Figure 7

Block diagram of future observatory system.

computers. More importantly, it will analyze the images immediately after they are observed. Thus we will be able to adjust the pointing, focus, exposure times, flash length, and observation list selection, in response to real time assessments of the night's sky conditions.

We are also preparing for the delivery of a new CCD detector, a Texas Instruments model VPCCD. This detector is reported to have better transfer efficiency and quantum efficiency than the current RCA CCD (Janesick *et al.*, in press). The TI CCD's 800 $\times$ 800 pixel format will make it easier to accurately measure the position of a star by oversampling the star image (i.e. spreading the images over more pixels), or alternatively to increase the number of background fiducial stars on short exposures by enlarging the field of view.

4. Analysis and Software

4.1. Overview

We analyze the data in four stages: 1) The preprocessing procedures move the raw data to the analysis computer in a usable format, and "clean" the images to remove non-astronomical features. 2) The image analysis programs find and analyze the stars in the image and write computer files recording coordinates, brightness, and shape. 3) The field comparison programs compare the star data for fields of stars observed on two different dates, and calculate the apparent motion of the Search List star. 4) Lastly, the postprocessing tasks collect calibration statistics, flag stars with significant apparent motion, and remove stars from the Search List that are no longer candidates.

Most of these outlined steps are carried out using a cluster of five VAX 8600 computers, operated by Lawrence Berkeley Laboratory's Computing Services division. For the image analysis we are using VISTA, a software system developed at the University of California's Lick Observatory (Lauer *et al.*, 1984). Our version of VISTA has been extensively modified to include analysis algorithms specific to our application, and to use the peripherals available at our site.

4.2. Preprocessing

Data Decoding and Transit

Typically a block of data from a single night is reduced at one time. This consists of 200-400 digitized images and bookkeeping records on Beta-format videotape. These ~50 Mbytes of data must be decoded, error checked, reformatted into a more useful computer standard, and moved to the VAX cluster for analysis. We use a PDP 11/44 computer to read the videotapes and reformat the results. We then transfer the data to the VAX cluster via traditional magnetic computer tapes.

This decoding and transporting process is time-consuming: 200 images take five hours to read into the PDP, two hours to write onto magnetic tapes, and another half hour to read into the VAX cluster. We are preparing an alternate data path, using the microVAX at the telescope to write the images on TK-50 magnetic tape cartridges. These will read directly into the VAX cluster via a microVAX on the Lawrence Berkeley Laboratory computer network.

Eventually we will perform the first two stages of data analysis at the telescope in real time, thus reducing the amount of data to be transported each observation night from ~50 Mbytes to ~0.05 Mbytes. This will be especially necessary with the Texas Instruments CCD, which collects almost four times as much data per observation.

Cleaning Images

For our purposes, a perfect image would be one in which any variation of electron counts from pixel to pixel would correspond to a variation in light intensity across the sky. The images we obtain are imperfect, primarily because of the following factors:

a) Dark Noise. Even in the dark, the potential wells of the CCD begin to collect electrons. Certain pixels and regions of the CCD are particularly "hot," and always register some electron counts. The CCD readout amplifier adds additional noise, usually seen as 60 Hz or 120 Hz stripes in the image with a peak-to-peak variation of about 200 electrons.

b) Flashed Background. The added background light from the flash unit is not perfectly uniform, as described in the previous chapter.

c) Vignetting. Due to the optical design, the intensity of light transmitted falls off sharply toward the edges of the field of view.

d) Quantum Efficiency Variation. The CCD pixels vary in their sensitivity to light by $\leq 2\%$ pixel-to-pixel.

The effects of the dark noise and the flash background are similar: both introduce extra electron counts varying from pixel to pixel, but constant (within poisson noise) from image to image. We remove these extra counts by subtracting from each image the pixel-by-pixel median of the three 1.5 second calibration

exposures. This median has only the counts in each pixel that are constant from image to image.

The vignetting and quantum efficiency can be corrected by a similar stratagem, since they both affect the pixel-to-pixel variation in sensitivity to light. The twilight sky provides a relatively flat light source, and thus the median of several twilight exposures gives a map of the responsiveness of each pixel to the same light level. From this map, we subtract the median of dark noise images obtained by reading out the unexposed dark CCD. The remaining image is then divided pixel by pixel into an observation exposure to correct the vignetting and quantum efficiency.

We can see the effect of these corrections graphically by plotting a histogram of the light intensities before and after each correction (see Figure 8). The histogram of Figure 8(b) suggests that the subtraction is correctly removing the extraneous electron counts from the image, leaving behind the star light plus the approximately gaussian noise of the counting statistics. The width of this almost-gaussian peak, $\sigma \approx 250$ electron counts, is consistent with the poisson noise expected after adding ~30,000 counts of flashed background to the image and then subtracting the flashed-background median frame. As an additional check of our ability to remove the background light, we display the subtraction of one medianed flash image from another and look for any systematic gradients of brightness. This subtraction has always appeared as a flat pattern of random noise, as we hoped.

Figure 8

Histograms of pixel intensities (in A/D counts):

(a) for typical star field with 1,000 A/D counts of flashed background;

(b) after subtracting median of three flashed calibration images from (a);

(c) after dividing (b) by twilight-sky quantum-efficiency map. Dotted line shows (b) for comparison.

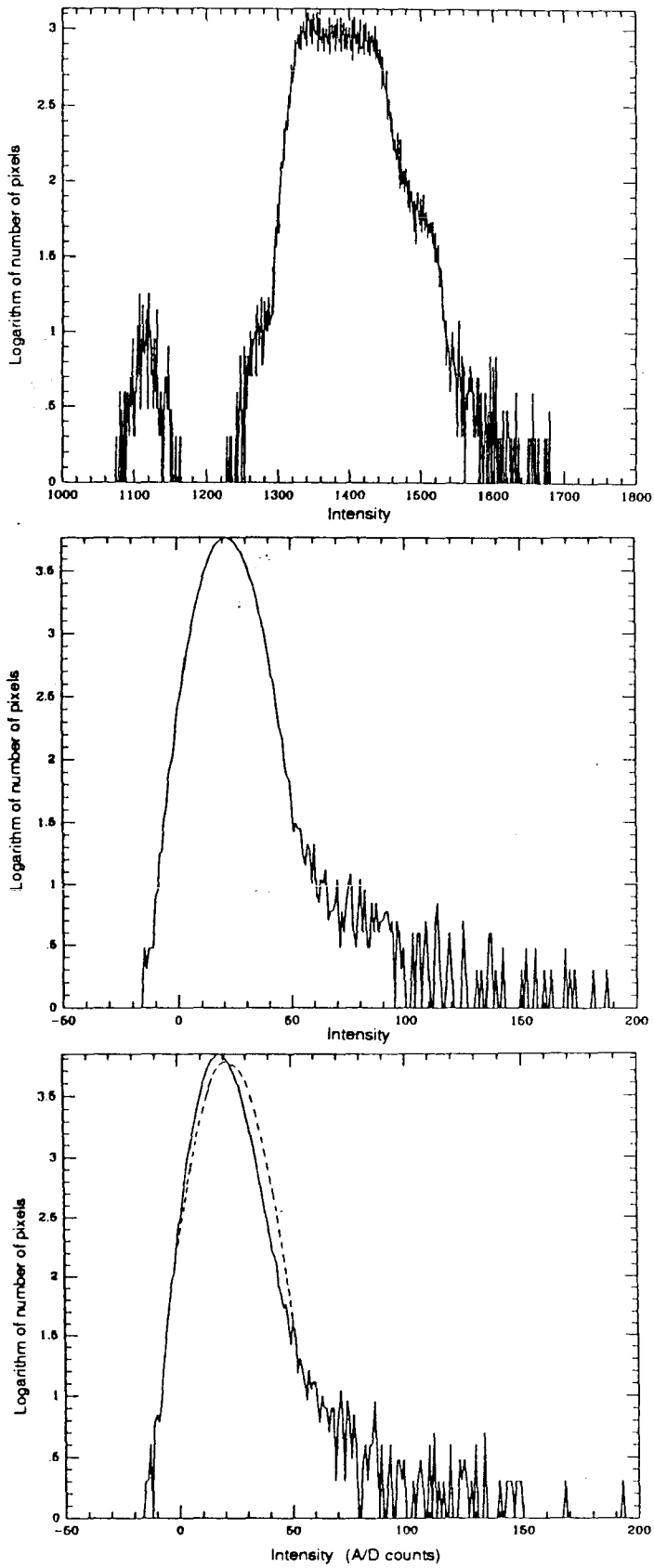

The vignetting and quantum efficiency correction do not greatly improve the image quality, as can be seen by comparing histograms (b) and (c) of Figure 8. We have found empirically that our star center-finding results are sensitive to the background correction, but not to the vignetting and quantum efficiency correction. Most of the image processing is done on images that have only been corrected for background light.

4.3. Image Analysis

Finding Stars

Once we have a "cleaned" image to work with, the next step of the analysis is to find all of the stars in the field. We only want stars bright enough to use as fiducial background stars for measuring the position of the Search List star; the brightness cutoff thus depends on the position accuracy for a given stellar brightness. A typical stellar image covers 4-5 pixels, with our 2.4 arcsec/pixel platescale. We can find the position of this image using the number of photoelectrons, S_1 and S_2, in the brightest two pixels in a given dimension. The x-coordinate position of the star is given by a function $x = f(r)$, where $r = S_1/S_2$ is the ratio of the brightest pixel counts, and the function $f(r)$ can be exactly calculated for any image point-spread-function (PSF). The accuracy of the location measurement is

$$\sigma_x = \frac{\partial f}{\partial r}\,\sigma_r$$

$$= \frac{\partial f}{\partial r}\, r \left[\left(\frac{N_1}{S_1}\right)^2 + \left(\frac{N_2}{S_2}\right)^2\right]^{1/2} \tag{8}$$

where we have used the signal-to-noise ratios S_1/N_1 and S_2/N_2 to calculate the error σ_r of the ratio r. King (1983) has shown numerically for a Gaussian PSF with an RMS width of ~1 pixel that $\partial f/\partial r \approx 1$ pixel. To first approximation, we use the signal-to-noise ratio S/N of a typical pixel near the peak of a star ($S/N \equiv S_1/N_1 \approx S_2/N_2$ and $r \approx 1$) and thus estimate the uncertainty of the star location to be $\sigma_x \approx N/S$ pixels.

If we only want fiducial stars that are located to better than 0.2 pixels, we must then look for stars with an intensity of $S = 5N$ counts above background. From the width of the gaussian in Figure 8(b), we know that the background noise is $N_b \approx 9$ A/D counts ≈ 250 electrons, while the signal poisson noise is $\sqrt{S}$. We have then

$$S = 5N = 5\sqrt{N_b^2 + S} \tag{9}$$

Solving for S, we find we are looking for stars with a brightness of $S \approx 1250$ electrons ≈ 45 A/D counts above background.

In finding and measuring the stars, we cannot assume that the background sky level is flat and uniform. The cleaning corrections are not perfect, clouds and haze may intrude, and an occasional cosmic ray may have gone through the CCD during the observation, filling a pixel or two with charge. We therefore

specifically search for *star-shaped* peaks 45 counts above the *local* background. We use an algorithm due to Stetson (1986). First the image is convolved with a two-dimensional function based on a gaussian of width matching the seeing for the night of observation. A constant is subtracted from the gaussian such that the integral under the convolution function is zero. Thus the convolution output is insensitive to changes in the local background. Surprisingly, it is also possible to normalize the convolution function so that the value of any point in the convolved image is equal to the amplitude of the gaussian that best fits the nearby pixels. We will use this gaussian amplitude, A_{gauss}, as the measure of a star's brightness throughout the following.

We scan the convolved image for values of $A_{gauss} \geq 45$ counts. When a possible star is found, two more tests screen its roundness and width before it is added to the list of confirmed stars. Stars with a roundness of $|R| > 1.0$ or a width differing from the seeing by more than a factor of two are rejected.

Center-finding

We have found that an iterative first-moment calculation gives a robust measure of the location of a star. First moments are, however, sensitive to the choice of background level, so we must first calculate a value for the local background around the star. We look at the pixels around the perimeter of a 7×7 box centered on the star's peak. For a gaussian of full width 2.4 pixels, this is in the region where the tail of the star is lost in the background. The analysis program

takes the median of these pixel values to obtain a robust measure of the background level.

After subtracting off this background from each pixel within the box centered on the peak of the star, the program proceeds to calculate the first-moment centroid. A new box of pixels is now centered on this centroid, and a new first moment centroid is calculated. The program iterates this last step until the centroid value converges. (If the program takes >6 iterations without converging, the star has an un-starlike shape, and we flag it as a bad fit.)

Star Description and Storage

The image analysis program also calculates other useful characteristics of each star in the field. A Star Data File is written for each image; it contains the following data for each star:

a) Row coordinate from first moment
b) Column "
c) Best fit gaussian amplitude
d) Peak pixel value
e) Summed brightness above background of pixels within radius=3
f) Roundness
g) Width
h) Amplitude of gaussian fit to three points in row
i) Width "
j) Amplitude of gaussian fit to three points in column
k) Width "

Some of these values are of frequent use, others are of occasional use, and some are helpful for diagnostics when a night's results prove unsatisfactory. One particularly useful value in the "occasional" category is the peak pixel value. A

value of 16,383 A/D counts indicates a saturated pixel (at the limit of the A/D converter) and thus flags the calculated centroid as unreliable.

4.4. Field Comparisons

Following the collection of two epochs of observations of the same star fields, and reduction of the images to create the Star Data Files, we are ready to compare the star fields. We begin by creating a list of matching stars for each star field pair. This list is corrected and pruned to contain only those stars useful in registering the two fields. We then fit the rotation, magnification, and offsets necessary to make the two fields match, and use the results of the fit to calculate the apparent motion of the Search List star. The following sections describe the details of this procedure.

Preparing the Matched Lists

We have found that stars that lie above row 400 on the CCD give poor results in the fitting procedures, because the vignetting in this region becomes so sharp that even the twilight-image correction leaves a poor image. Similarly, saturated stars, with more than 16,383 A/D counts in their peak pixel, result in poor fits. Before matching the fields, we delete these stars. The field comparison program then finds matches between the two epochs, for the remaining stars. The matching is accomplished by an exhaustive search through all possible matchings of stars. This is a reasonably efficient algorithm for our lists, which are both ordered by increasing row coordinate. Typically, one of the first few

match attempts is correct, with epoch-to-epoch partners found for >75% of the stars.

At this stage, we also make a correction to the star coordinates to account for the pincushion optical distortion $\Delta r = p_0 r^3$, where r is the distance from the optical center at (Column 140, Row 234). If a star is located at r_1 in the first-epoch image and at r_2 in the second-epoch image, then the differential pincushion distortion, which the program corrects, is

$$\begin{aligned} \Delta_{differential} &= p_0(r_1^3 - r_2^3) \\ &\approx p_0 r_1^2 \delta r \end{aligned} \tag{10}$$

where $\delta r = r_1 - r_2$ is the measure of the mismatch in telescope pointing between the two epochs. For our optical system we have measured the pincushion constant to be $p_0 = 6.5\times10^{-8} \pm 4.5\times10^{-8}$ pixels^{-2}. We estimate the systematic error, $\sigma_{pincushion}$, introduced by the uncertainty in the pincushion constant, $\delta p_0 = 4.5\times10^{-8}$ pixels^{-2} to be

$$\begin{aligned} \sigma_{pincushion} &= \frac{\partial \Delta_{differential}}{\partial p_0} \delta p_0 \\ &= r_1^2 \delta r \, \delta p_0 \end{aligned} \tag{11}$$

With the RMS pointing error δ= 6 pixels, and a typical distance r = 160 pixels of a fiducial star from the optical center, we find the systematic error introduced by the corrected pincushion to be approximately $\sigma_{pincushion} \approx 0.01$ pixels.

Field Fitting

The field comparison program next goes twice through a night's worth of matched lists. The first time through, a "downhill simplex" fitting algorithm [see Press *et al.* (1986)] finds the values of four parameters, rotation, magnification, row offset and column offset, that best align each pair of star fields. (The fitting algorithm weights each star in the field by its brightness.) We use the global average of all of the magnification and rotation values to describe the difference in conditions at the telescope between the two nights. The second time through the matched lists the fitting program finds individual values for the row and column offsets between the star fields, but uses the global average of magnification and rotation in its calculations. This two parameter fit is less affected by outliers and sparse fields with few fiducial stars.

We would like to do this fitting procedure leaving out the Search List star. The Dearborn Catalog, however, gives coordinates that can be inaccurate by as much as 3 arcminutes $\approx$ 75 pixels, and there may be more than one likely bright star within this radius of error. Our solution is to perform the field fitting once for each likely bright star near the center of the image. The program leaves the likely star out of the fit, and then uses the resulting fit parameters to measure the apparent motion, m_a, of the likely star. The extra inadvertent measurements of stars which are not on our Search List does not reduce the probability of finding a companion star; they simply provide extra calibration points as distant stars which do not move.

4.5. Postprocessing

Candidate Selection and Rejection

Thus we reach the primary goal of the analysis: we have measured the apparent motion of each Search List star (plus a few inadvertent extras). The last step is to dispose of each Search List star according to its measured m_a. We delete candidates with small m_a from the Search List (using criteria described in Section 5.3), and re-examine the stars which are in the outskirts of the motion distribution. Generally none of these (except one) should come close to the amount of motion expected for a star closer than 0.8 pc, but they will allow us to eliminate systematic errors in our experiment. Improvements of the experiment should seek to improve the precision of our measurement of apparent motion. This will reduce the time required between first- and second-epoch observations.

Candidate Follow-up Studies

When and if we do find a star with m_a of the magnitude and direction appropriate for a nearby star, we will check our result in a few ways. First, we will follow its motion for a longer time, and if it follows the expected path in the sky this would be conclusive proof of its distance. For immediate confirmation, we will take photometric exposures with different color filters. The colors can distinguish between red dwarf stars and red giant stars in certain cases (Penfold, 1978). We will also obtain spectra at Lick Observatory, and look for the characteristic bands which differentiate dwarfs from giants.

These measurements will test whether the star is nearby, but not whether it is orbiting the Sun. We will need to measure the radial velocity and the proper motion to determine the orbital parameters. The radial velocity can be obtained from the spectra taken at Lick Observatory. The minimum annual proper motion, $\mu(r_{\max}) \approx 0.01$ arcseconds, is well below the detection threshold of our parallax measurements, so we will probably measure μ using an astrometric program at another observatory. However, if the star happens to be very close, or the new Texas Instruments CCD gives much better performance, we may be able to measure μ at the Leuschner telescope.

5. Results and Discussion

5.1. Calibration Results

Table 3 describes the observations used for calibration measurements. The precision of our parallax measurement can be seen in the distribution of apparent motion, m_a, that we find for stars that are not expected to move. Figure 9 shows this distribution for stars observed twice on the night of 8 August 1986, approximately one hour apart.

Table 3
Calibration Observations

List Name	Date	Time Range *Universal Time*	Airmass Range $sec(\theta_{zenith})$	Seeing *arcseconds*
Aug I	8 August 1986	05:59—06:36	1.01—1.22	~3
Aug II		06:48—07:25	1.04—1.28	
Oct I	13 October 1986	02:30—03:14	1.05—1.29	~1.5
Oct II		03:18—04:02	1.13—1.44	

We expect no parallactic motion in one hour, so the scatter around $m_a = 0$ in both the row and column directions gives us an estimate of the error of our measurement. The RMS deviations about the mean are $\sigma_{m_a} = \sigma_{Row} = \sigma_{Column} = 0.063$ pixels, with a sample size of $N = 60$ star fields. (For the plate scale of 2.4

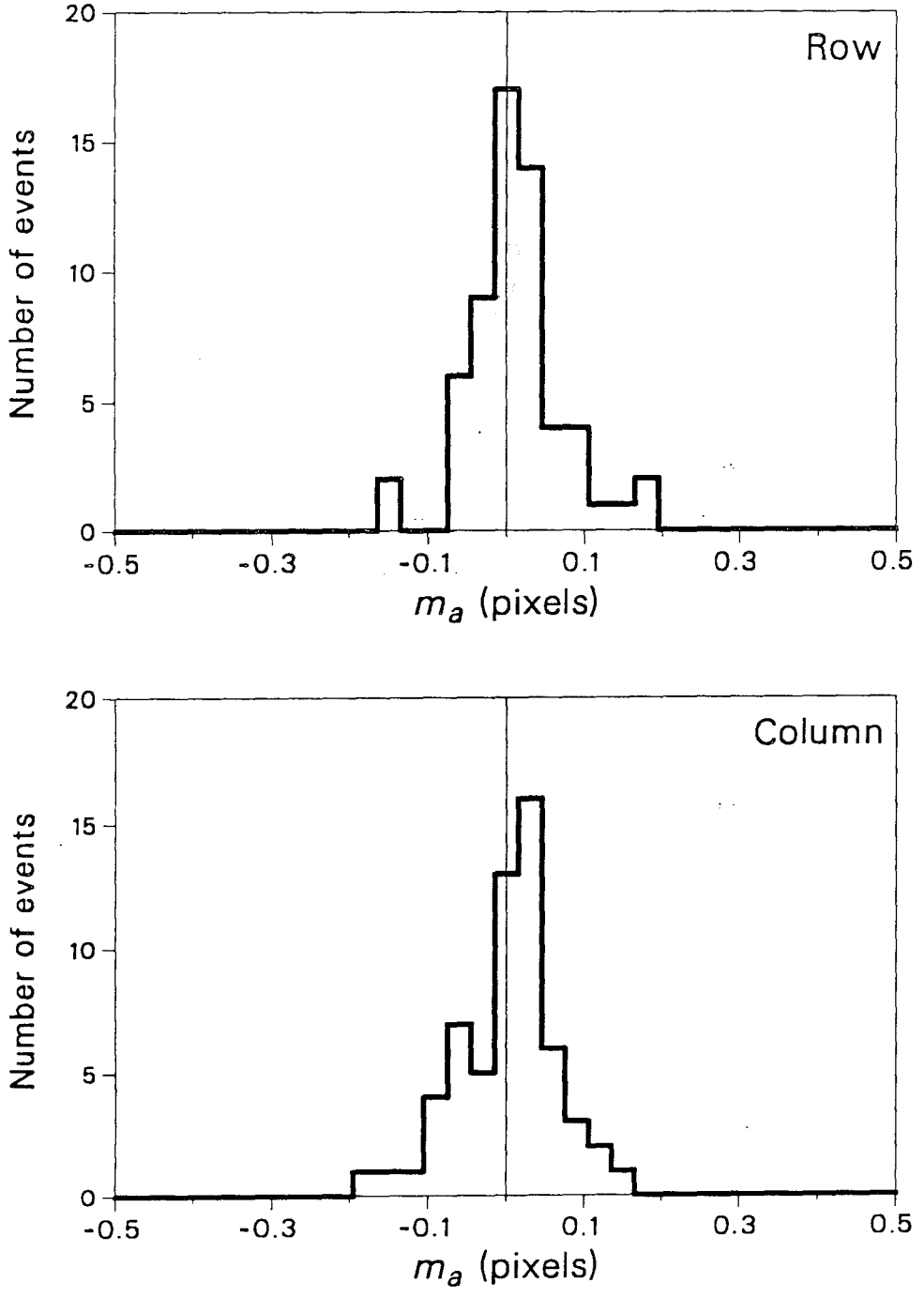

Figure 9

Apparent motion, m_a, for Aug I list matched with Aug II list.

arcseconds per pixel, this corresponds to $\sigma_{m_a} = 0.15$ arcseconds.) The furthest outliers from zero motion are at $\Delta_{Row} = \Delta_{Column} = 0.19$ pixels. Figure 10 shows similar results for a subset of the same set of stars also observed twice the same night but two months later, on October 13, 1986. For this histogram,

$$\begin{aligned} \sigma_{Row} &= 0.064 \text{ pixels} \\ \sigma_{Column} &= 0.052 \text{ pixels} \\ \Delta_{Row} &= 0.16 \text{ pixels} \\ \Delta_{Column} &= 0.14 \text{ pixels} \end{aligned} \tag{12}$$

for $N = 42$ star fields. We see that the distributions have a similar scatter under different observation conditions: the atmospheric seeing on the August night was about twice that of the October night.

The accuracy of the measurements of m_a is indicated by the mean of these distributions. We expect $<m_a> = 0$ for stars observed twice on the same night. We find for the August night,

$$\begin{aligned} <m_a>_{Row} &= 0.011 \pm 0.008 \text{ pixels} \\ <m_a>_{Column} &= 0.002 \pm 0.008 \text{ pixels} \end{aligned} \tag{13}$$

and for the October night,

$$\begin{aligned} <m_a>_{Row} &= -0.021 \pm 0.010 \text{ pixels} \\ <m_a>_{Column} &= 0.021 \pm 0.008 \text{ pixels} \end{aligned} \tag{14}$$

There is some bias apparent in the October data, but it is small compared to σ_{m_a}, which determines the smallest m_a the search can detect.

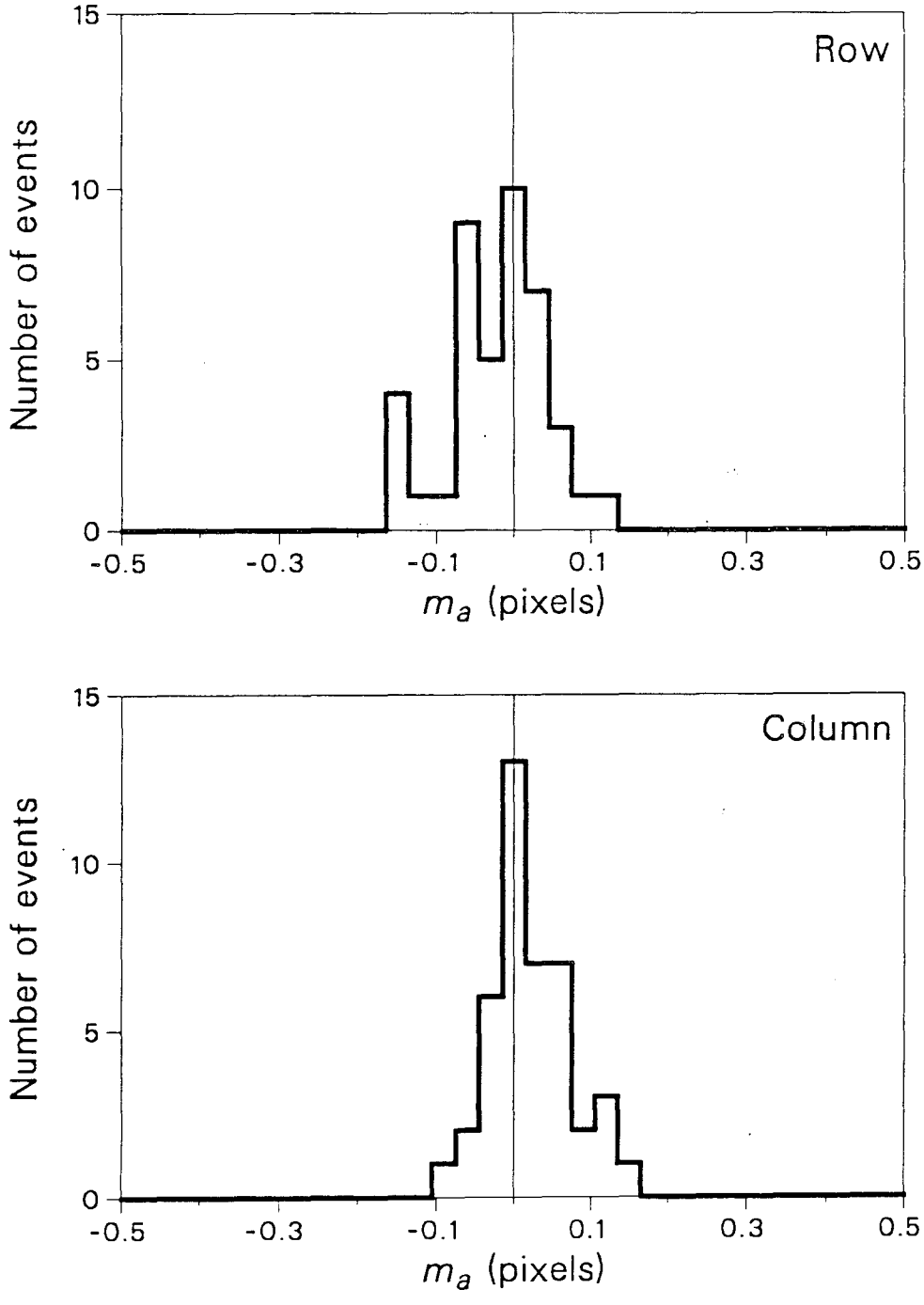

Figure 10

Apparent motion, m_a, for Oct I list matched with Oct II list.

The overall measurement precision of m_a is best seen in the distribution of m_a found for stars measured two months apart, as shown in Figure 11. This distribution tests the entire data collection and analysis procedure. The mean apparent motion is near zero:

$$<m_a>_{Row} = -0.008 \pm 0.010 \text{ pixels}$$

$$<m_a>_{Column} = 0.030 \pm 0.010 \text{ pixels} \quad (15)$$

For these $N = 41$ stars, we have the following deviations:

$$\sigma_{Row} = 0.080 \text{ pixels}$$

$$\sigma_{Column} = 0.071 \text{ pixels} \quad (16)$$

$$\Delta_{Row} = \Delta_{Column} = 0.18 \text{ pixels}$$

5.2. Error Analysis

Systematic Errors

There are a number of sources of systematic error, $\sigma_{systematic}$, at the level of ~0.03 pixels. The transfer inefficiency of the CCD, for example, may not allow more precise measurements, even with the improvement due to flashing the CCD with background light. If the inefficiency changes from $\epsilon = 0.0001$ in the first epoch to $\epsilon = 0.0002$ in the second (corresponding to a temperature change of about 10 degrees), the amount of charge in the tails of a star image at (Row 512, Column 320) changes from 8% to 15%. This would shift the centroid by

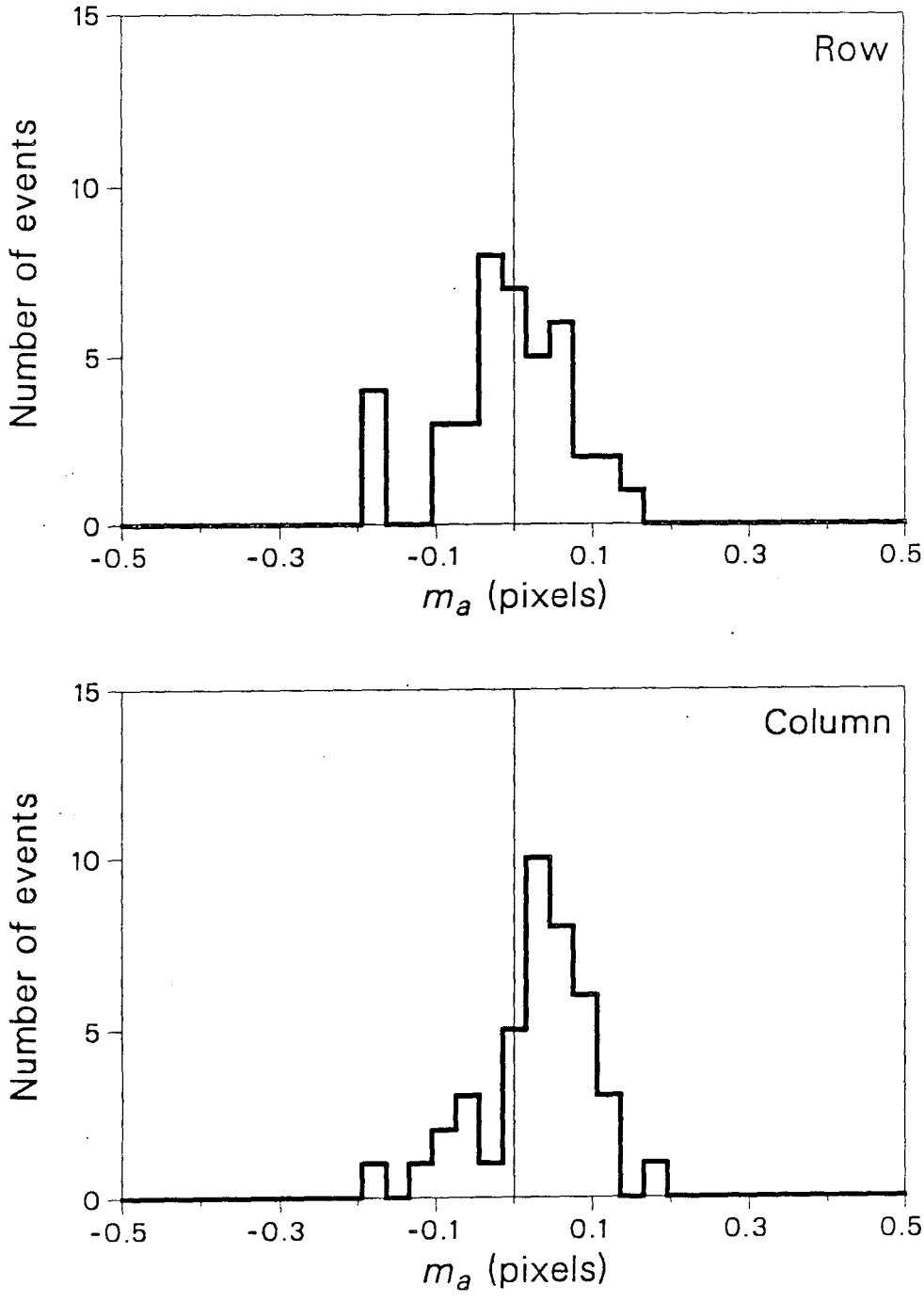

Figure 11

Apparent motion, m_a, for Aug II list matched with Oct I list.

$\sigma_{ineffic} \approx$ (0.15—0.08) pixels $\approx$ 0.03 pixels.

As discussed in Section 4.4, the pincushion distortion also contributes an error on the order of $\sigma_{pincushion} \approx 0.01$ pixels. Evidence for this source of error is the increase in m_a for fields with poorly matched pointing ($\geq$ 12 pixels) between two epochs. The pincushion error can, however, be removed by fitting the pincushion parameter, p_0, to the data set taken as a whole.

We thus estimate the overall systematic error to be

$$\sigma_{systematic} \approx (\sigma^2_{ineffic} + \sigma^2_{pincushion})^{1/2} \approx 0.032 \qquad (17)$$

This is adequate for the search for a Companion. If more precision is needed for a different search design, these sources of error would have to be studied further. In particular, it would be important to understand if the $<m_a>$ bias and $\sigma_{systematic}$ are due to the same source.

Statistical Errors

The m_a distributions shown in Figures 9, 10, and 11 are clearly not simple gaussians drawn from a single normal distribution. They can be approximately described as the sum of gaussians drawn from a family of normal distributions, where the widths of the distributions depend on a number of contributing sources of error. The two dominant statistical sources of error are a) the centroid uncertainty, $\sigma_{centroid}$, a function of the brightness, A_{gauss}, of a star, and b) the number of background fiducial stars, $N_{fiducial}$, in the field. These two factors are correlat-

ed, since both A_{gauss} and $N_{fiducial}$ increase with increasing exposure time. For large $N_{fiducial}$, both of these sources of statistical error become negligible, and the overall measurement error reaches a minimum at $\sigma_{systematic}$.

Determining $\sigma_{centroid}$

Figure 12 shows the dependence of $\sigma_{centroid}$ on brightness, by plotting the residual deviations of star coordinates from the overall fit against A_{gauss}. The plot includes fields with more than $N_{fiducial} = 20$ stars, and with telescope pointing matched to within 9 pixels for the two epochs. We expect these epoch-to-epoch deviations, σ_{e-e}, between two stars to be given by

$$\sigma_{e-e} = \sqrt{2\,\sigma^2_{centroid} + \sigma^2_{systematic}} \tag{18}$$

where $\sigma_{centroid}$ is the individual standard deviation of each centroid measurement, and the factor of 2 accounts for the two measurements made, in the first and second epoch.

Improving on the estimate of Section 4.3, we will take $\sigma_{centroid} \approx N/S_2$, where we use S_2, the signal of the second brightest pixel, rather than the amplitude of the star's gaussian in the signal-to-noise calculation. This choice reflects the fact that a star's location on the pixels is determined roughly by the ratio of the counts in the two neighboring brightest pixels, and this ratio's uncertainty is dominated by the uncertainty of the less bright pixel. For stellar gaussians with amplitude A_{gauss} (in electrons) and FWHM ≈ 2.5 pixels, we find $S_2 \approx A_{gauss}/2$.

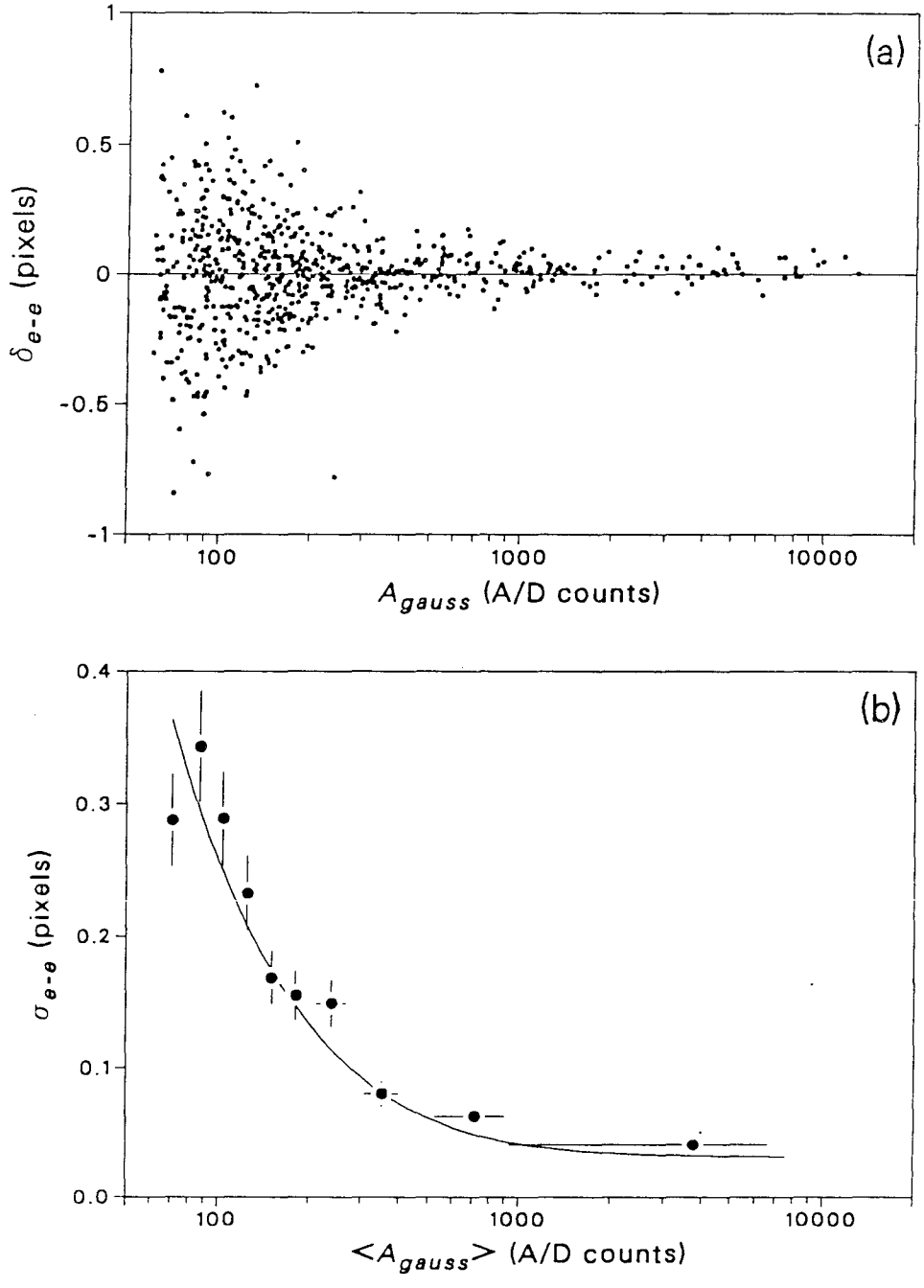

Figure 12

For Aug I list matched with Aug II: (a) the residual epoch-to-epoch deviation, δ_{e-e}, in column coordinate vs. the brightness of the star, A_{gauss}, for all stars in a field after correcting for fit offset, magnification, and rotation; (b) standard deviation, σ_{e-e}, for residuals in (a), averaging every 69 stars binned in order of increasing A_{gauss}.

Thus

$$\sigma_{e-e}^2 = 2\,\frac{N^2}{S_2^2} + \sigma_{systematic}^2$$

$$= 2\,\frac{(A_{gauss}/2) + N_b^2}{(A_{gauss}/2)^2} + \sigma_{systematic}^2 \qquad (19)$$

where $N_b = 300$ electrons is the background noise. The solid line in Figure 12 shows σ_{e-e} plotted against A_{gauss}. The consistency of this curve with the empirical results indicates that $\sigma_{centroid} \approx N/S_2$ is a reasonable estimate. In the following analysis, we will use this estimate for the centroid uncertainty, σ_{search}, of the Search List star, and for the centroid uncertainty, $\sigma_{fiducial}$, of the fiducial stars.

Number of Fiducial Stars

We can now write the m_a-measurement error, σ_{m_a}, for a field with $N_{fiducial}$ fiducial stars, as

$$\sigma_{m_a} = \left(2\,\frac{\sigma_{fiducial}^2}{N_{fiducial}} + \sigma_{systematic}^2 + 2\sigma_{search}^2\right)^{1/2}$$

$$\approx \left(2\,\frac{(A_{fiducial}/2)+N_b^2}{N_{fiducial}\,(A_{fiducial}/2)^2} + \sigma_{systematic}^2\right)^{1/2} \qquad (20)$$

where $A_{fiducial}$, the fiducial star brightness, is itself dependent on $N_{fiducial}$, since longer exposures give larger $N_{fiducial}$ and brighter fiducial stars. This dependence is shown in Figure 13. We neglect σ_{search}, the uncertainty of the Search List star's centroid, because it is much smaller than $\sigma_{systematic}$. The solid curves in

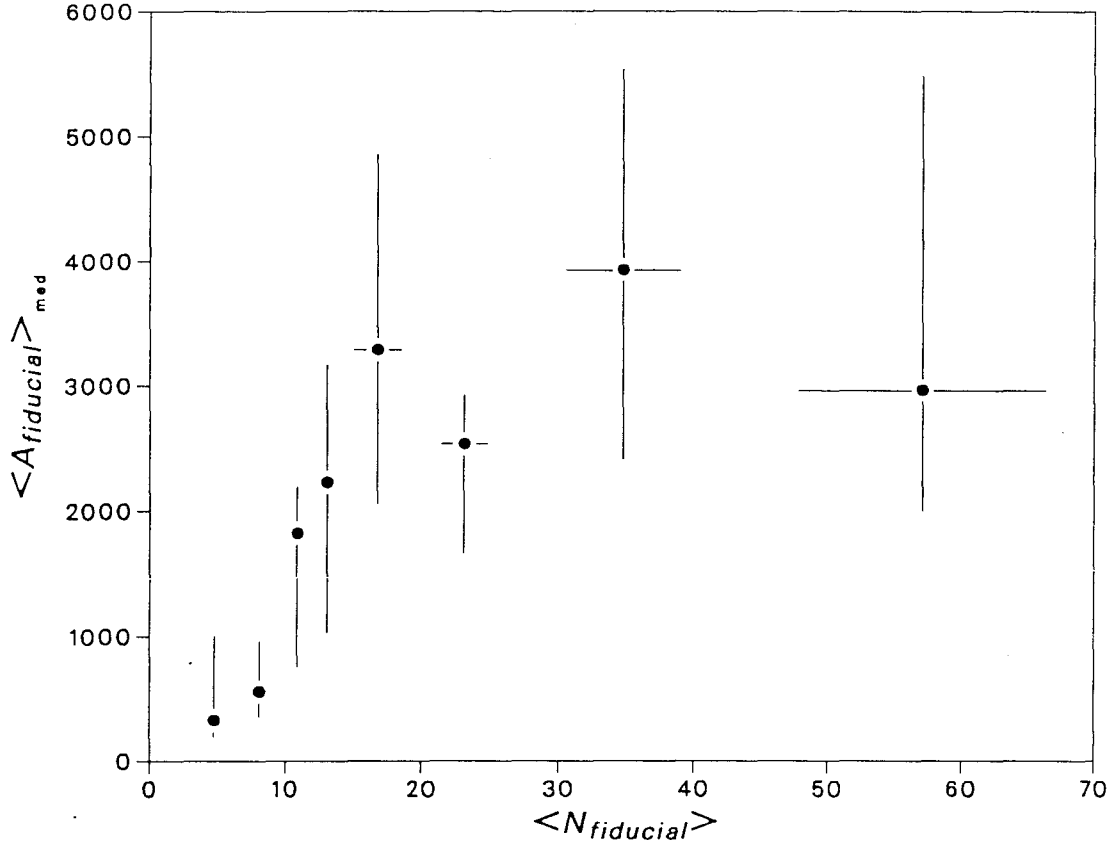

Figure 13

Brightest fiducial star amplitude, $A_{fiducial}$, vs. number of fiducial stars, $N_{fiducial}$, for 72 fields binned by 9 in order of increasing $N_{fiducial}$. The median of the 9 fields' $A_{fiducial}$ is plotted.

Figures 14 and 15 show the expected σ_{m_a} plotted against $N_{fiducial}$. The small underestimate of the error can be accounted for by our use of the brightest fiducial star rather than a weighted average of all of the fiducial stars.

5.3. Search Strategy

With this understanding of the measurement precision, we have chosen a search strategy that minimizes the chance of missing a nearby star on the Search List, and also minimizes the time required to complete the search.

Dim Stars: Long Exposures

Dim Search List stars require long exposures, and thus have more fiducial stars available. For those stars with more than ten background fiducial stars visible in the same field, we find that any parallactic motion greater than $m_\pi = 2\Delta_{Row,Column} \approx 0.4$ pixels would be clearly distinguishable from the zero motion stars shown in Figure 11. This value of m_π lies at ~5σ for $N_{fiducial} \geq 10$, based on the deviation shown in Figures 14 and 15. For these long-exposure stars, two epochs separated by two months gives a little more than $m_\pi = 0.4$ pixels for stars undergoing their maximum parallactic motion. In Figure 16, the distribution of m_a for Aug II matched with Oct I is replotted to show this expected two-month motion and the six-month peak-to-peak motion, $(m_\pi)_{p-p}$.

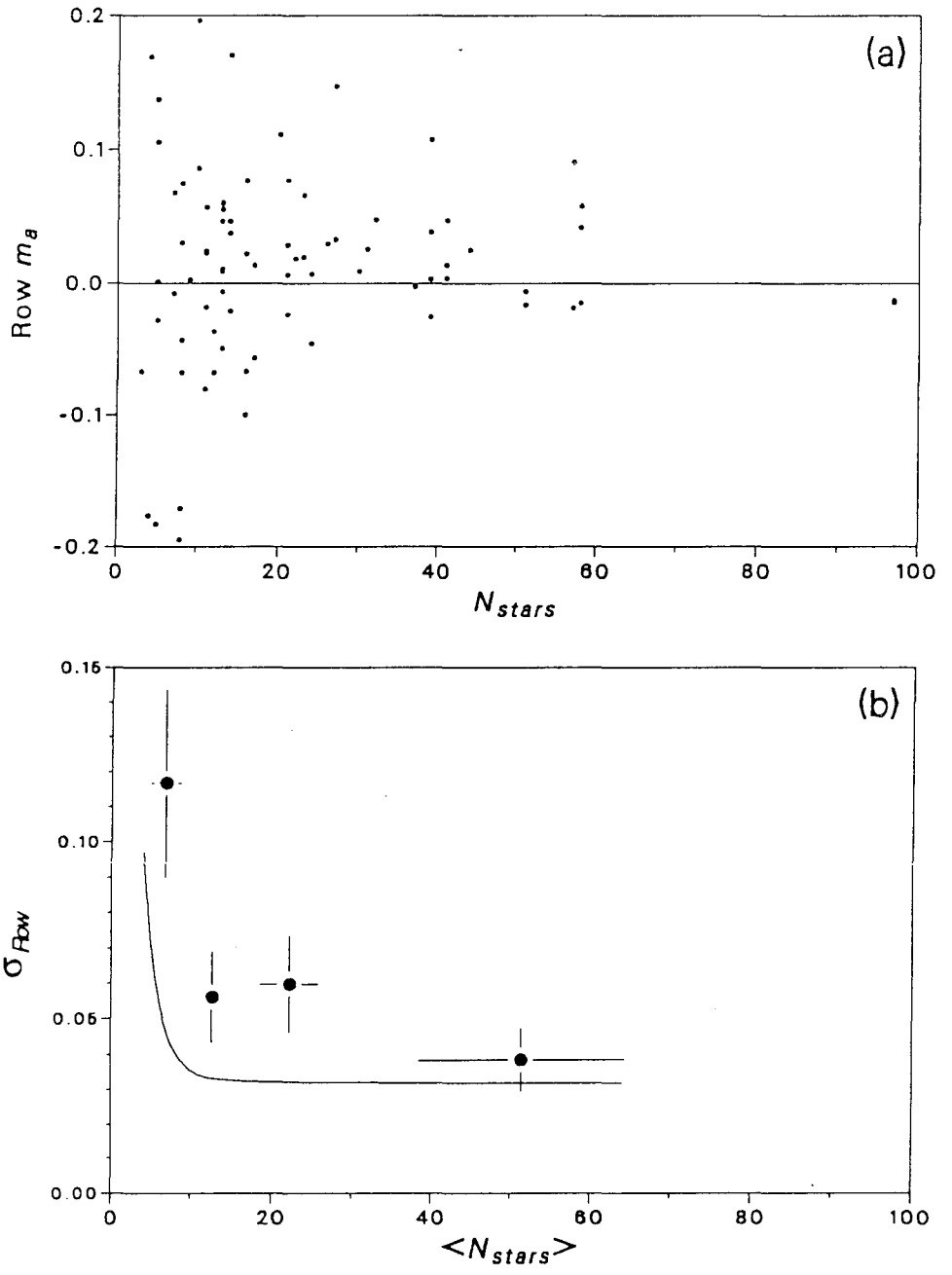

Figure 14

For Aug I list matched with Aug II: (a) the apparent motion, m_a, in row coordinate vs. the number of fiducial stars, $N_{fiducial}$; (b) standard deviation, σ_{row}, for apparent motion in (a), averaging every 20 stars binned in order of increasing $N_{fiducial}$.

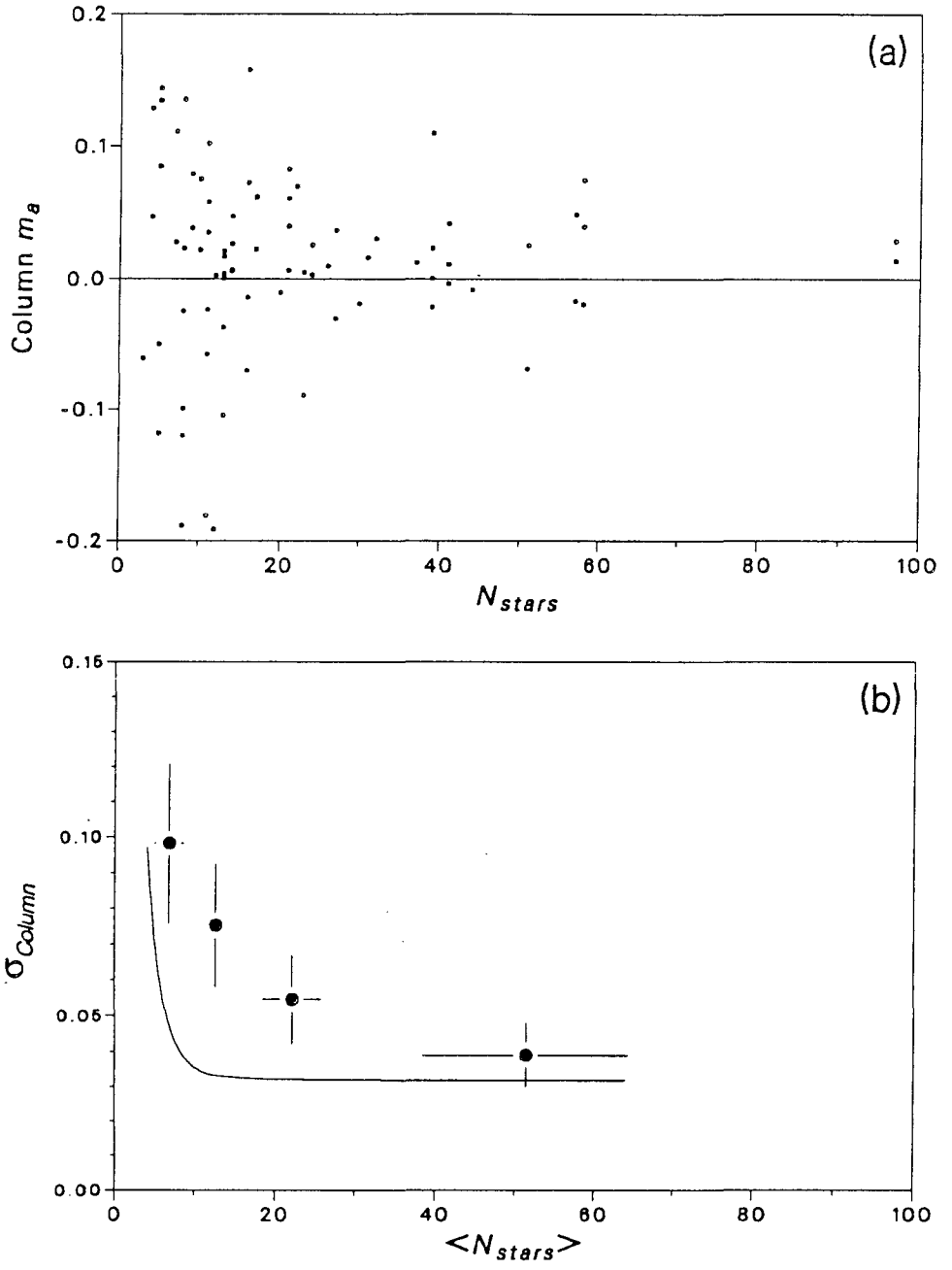

Figure 15

For Aug I list matched with Aug II: (a) the apparent motion, m_a, in column coordinate vs. the number of fiducial stars, $N_{fiducial}$; (b) standard deviation, σ_{column}, for apparent motion in (a), averaging every 20 stars binned in order of increasing $N_{fiducial}$.

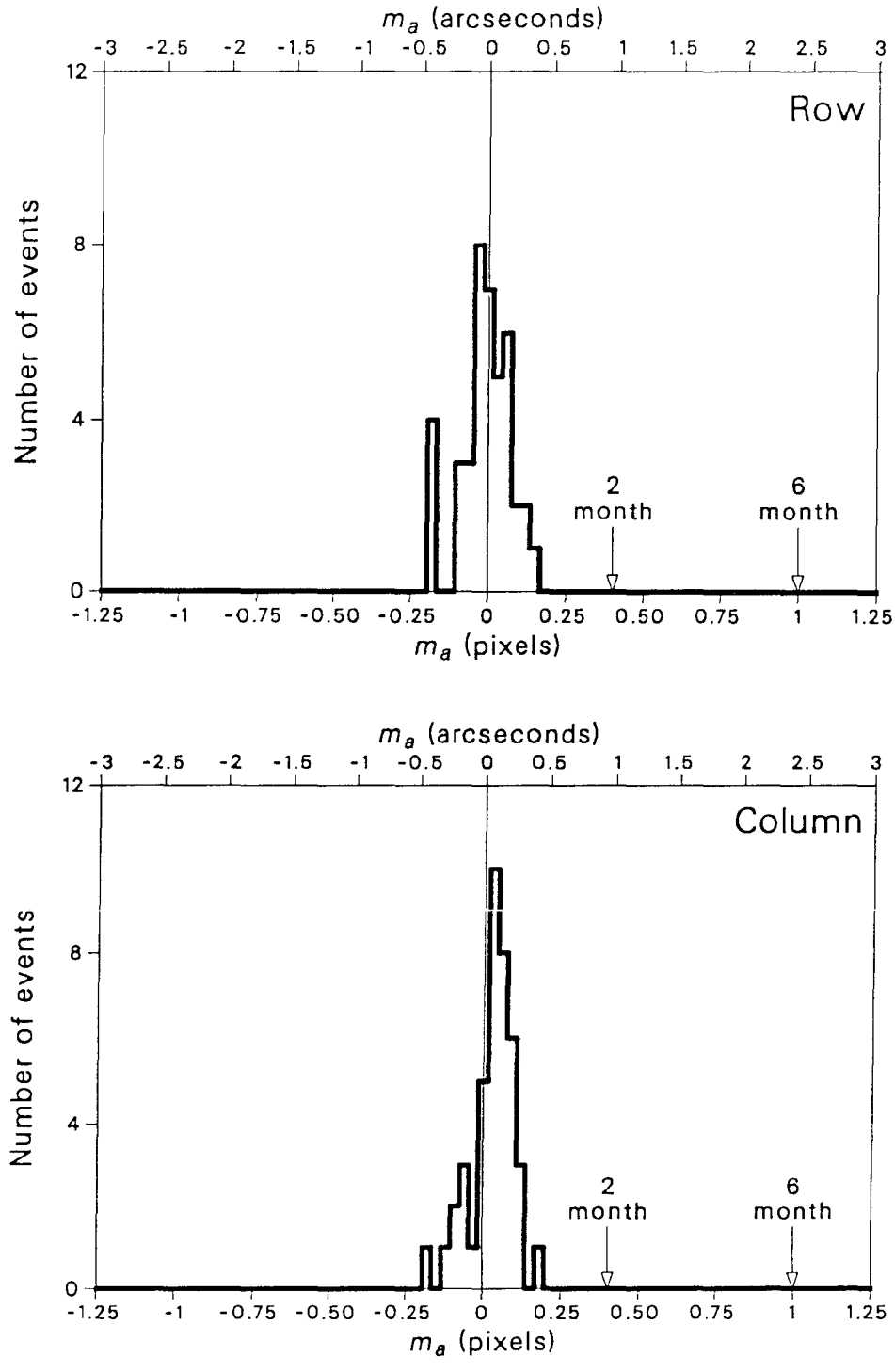

Figure 16

Apparent motion, m_a, for Aug II list matched with Oct I list. The arrows indicate the average *magnitude* of a) the expected parallactic motion, m_π, for this two-month time interval, and b) the six-month peak-to-peak motion, $(m_\pi)_{p-p}$. The *direction* of motion depends on the ecliptic coordinates of the measured star.

Bright Stars: Short Exposures

Bright Search List stars require short exposures and thus have fewer fiducial stars available. We handle these stars as follows.

a) For the stars with at least one fiducial star, we will allow a longer time interval to pass between the epochs. If necessary, the entire six-month peak-to-peak parallax, $(m_\pi)_{p-p} \geq 1$ pixel, can be used.

b) Search List stars with no fiducial stars in the field present a problem of dynamic range. We will take multiple exposures of a bright star without moving the telescope, reading out the CCD between each exposure. Stacking the images in software then increases the effective exposure time without saturating the image of the bright star. This brings fainter fiducial stars above the noise.

Both of these strategies will be obviated when the Texas Instruments CCD is incorporated into the system. The two- to three-fold increase in dynamic range will bring more fiducial stars above the background noise before a bright star saturates the CCD. The 800×800 pixel format will also allow us to share the star light of the bright star among more pixels, and/or use a larger field of view containing more fiducial stars.

For the Aug I and Aug II lists, the Search List stars with fewer than one fiducial star in the field account for less than 5% of the Search List. However, since these stars are the brightest in the Search List and the Companion could be a very close star, it is important that we include them in the Search.

6. Conclusion

The above results and analysis demonstrate that the Companion Star Search can accomplish its goals. The 41 stars used as a calibration in Figure 16 also represent the beginning of the Companion Search. The measured values of m_a for these stars indicate that none of these stars is a nearby companion. We are currently observing the remaining 2,729 stars on the Search List, and expect to complete the observations within the next year. We hope that this time span is cut short by the discovery of a Companion.

7. References

Abt, H. A. (1983). Normal and abnormal binary frequencies. *Ann. Rev. Astron. Astrophys.*, **21**, 343-72.

Alvarez, L. W., W. Alvarez, F. Asaro, and H. V. Michel (1980). Extraterrestrial cause for the Cretaceous-Tertiary extinction. *Science*, **208**, 1095-1108.

Alvarez, W. and R. A. Muller (1984). Evidence from the crater ages for periodic impacts on the earth. *Nature*, **308**, 718-720.

Alvarez, W. (1986). Toward a theory of impact crises. *EOS*, **67**, no. 35, 649, 653-655, 658.

Bahcall, J. N. and R. M. Soneira (1980). The universe at faint magnitudes. I. Models for the Galaxy and predicted star counts. *Astrophys. J. Suppl.*, **44**, 73.

Bahcall, J. N. (1986). Brown Dwarfs: Conference Summary. In *Astrophysics of Brown Dwarfs*, ed. M. C. Kafatos, R. S. Harrington and S. P. Maran, pp. 233-237. Cambridge: Cambridge University Press.

Burns, M. S. (1985). Development of a CCD Camera for an Automated Supernova Search and Observations of a Supernova in NGC 5033. LBL-20648, Lawrence Berkeley Laboratory, Berkeley, CA. Ph.D. Thesis.

Davis, M., P. Hut, and R. A. Muller (1984). Extinction of species by periodic comet showers. *Nature*, **308**, 715-717.

Hoffleit, D. (1982). *The Bright Star Catalogue*, Fourth revised edition. New Haven: Yale University Observatory. With the collaboration of C. Jaschek.

Hut, P. (1984). How stable is an astronomical clock which can trigger mass extinctions on the earth? *Nature*, **311**, 638-641.

Hut, P. (1985). Evolution of the solar system in the presence of a solar companion star. In *The Galaxy and the Solar System.* Proceedings of conference, Tucson, Arizona, January 1985, to be published.

Janesick, J. R., T. Elliott, S. Collins, and H. Marsh (in press). The future scientific CCD. *SPIE.*

Kare, J. T. (1984). An Automated Search for Supernovae. LBL-19340, Lawrence Berkeley Laboratory, Berkeley, CA. Ph.D. Thesis.

Kare, J. T., M. S. Burns, F. S. Crawford, P. G. Friedman, R. A. Muller, C. R. Pennypacker, and S. Perlmutter (to be published). An automated search for supernova explosions.

King, I. R. (1983). Accuracy of measurement of star images on a pixel array. *P.A.S.P.*, **95**, 163-168.

Lauer, T., R. Stover, and D. Terndrup (1984). The VISTA Programmer's Guide, Version 2. Technical Reports No. 34, University of California, Lick Observatory.

Lee, O. J., R. J. Baldwin, and D. W. Hamlin (1943). *Annals Dearborn Observatory*, **V**. Part 1A.

Lee, O. J. and T. J. Bartlett (1944). *Annals Dearborn Observatory*, **V**. Part 1B.

Lee, O. J., G. D. Gore, and T. J. Bartlett (1947). *Annals Dearborn Observatory*, **V**. Part 1C.

Luyten, W. J. (1979;1980). *NLTT Catalogue*. Minneapolis: University of Minnesota. (4 vols.)

Muller, R. A. (1985). Evidence for Nemesis: a solar companion star. LBL-20438, Lawrence Berkeley Laboratory. Also in Proceedings of *The Galaxy and the Solar System*, Tuscon, Arizona.

Nagy, T. A. (1979). Report no. R-SAW-8/79-01, Systems and Applied Sciences Corporation.

Penfold, J. E. (1978). Observations of faint red stars at intermediate galactic latitude. *Mon. Not. R. Astr. Soc.*, **182**, 283-291.

Press, W. H., B. P. Flannery, S. A. Teukolsky, and W. T. Vetterling (1986). *Numerical Recipes*, p. 289. Cambridge University Press.

Rampino, M. R. and R. B. Stothers (1984). Terrestrial mass extinctions, cometary impacts and the Sun's motion perpendicular to the galactic plane. *Nature*, **308**, 709-712.

Raup, D. M. and J. J. Sepkokski, Jr. (1984). *Proc. Nat. Acad. Sci. U.S.A.*, **81**, 801-805.

Schaifers, K. and H. H. Voigt (1982). Astronomy and Astrophysics. In *Landolt-Bornstein: New Series*, ed. K.-H. Hellwege, vol. 2, p. b.25. Berlin: Springer-Verlag.

Shapiro, S. L. and S. A. Teukolsky (1983). *Black Holes, White Dwarfs, and Neutron Stars.* New York: Wiley.

Shoemaker, E. M. (1985). In *The Galaxy and the Solar System.* Proceedings of conference, Tucson, Arizona, January 1985, to be published.

Stetson, P. B. (1986). *DAOPHOT User Manual.* Victoria, British Columbia: Dominion Astrophysical Observatory. Computer program package for photometry.

Stevenson, B. (1984). Private communication.

Reynolds, R. T., J. C. Tarter, and R. G. Walker (1980). A proposed search of the solar neighborhood for substellar objects. *Icarus*, **44**, no. 3, 772-779.

Toon, O. B., J. B. Pollack, T. P. Ackerman, R. P. Turco, C. P. McKay, and M. S. Liu (1982). Evolution of an impact-generated dust cloud and its effects on the atmosphere. *Geol. Soc. Am. Special Paper 190*, 187-200.

Turco, R. P., O. B. Toon, T. P. Ackerman, J. B. Pollack, and C. Sagan (1983). Nuclear winter: Global consequences of multiple nuclear explosions. *Science*, **222**, 1283.

Whitmire, D. P. and A. A. Jackson (1984). Are periodic mass extinctions driven by a distant solar companion? *Nature*, **308**, 713-715.

Whitmire, D. P. and J. J. Matese (1985). Periodic comet showers and Planet X. *Nature*, **313**, 36-38.

van de Kamp, P. (1982). Evolutionary trends in wide binaries. In *Binary and Multiple Stars as Tracers of Stellar Evolution*, ed. Z. Kopal and J. Rahe, pp. 81-103. Dordrecht: Reidel.